



Published in final edited form as:

Nature. 2016 November 24; 539(7630): 570–574. doi:10.1038/nature20141.

Macrophages redirect phagocytosis by non-professional phagocytes and influence inflammation

Claudia Z. Han^{1,2}, Ignacio J. Juncadella¹, Jason M. Kinchen¹, Monica W. Buckley^{1,2}, Alexander L. Klibanov^{3,4}, Kelly Dryden⁵, Suna Onengut-Gumuscu^{6,7}, Uta Erdbrügger⁸, Yun M. Shim³, Kenneth S. Tung^{3,9}, and Kodi S. Ravichandran^{1,2}

¹The Center for Cell Clearance

²Department of Microbiology, Immunology, and Cancer Biology, University of Virginia, Charlottesville, Virginia, USA

³Department of Medicine, University of Virginia, Charlottesville, Virginia, USA

⁴Robert M. Berne Cardiovascular Research Center, University of Virginia, Charlottesville, Virginia, USA

⁵Department of Molecular Physiology and Biological Physics, University of Virginia, Charlottesville, Virginia, USA

⁶Department of Medicine, Division of Endocrinology and Metabolism, University of Virginia, Charlottesville, Virginia, USA

⁷Center for Public Health Genomics, University of Virginia, Charlottesville, Virginia, USA

⁸Department of Medicine, Division of Nephrology, University of Virginia, Charlottesville, Virginia, USA

⁹Department of Pathology, University of Virginia, Charlottesville, Virginia, USA

Abstract

Professional phagocytes (such as macrophages^{1,2}) and non-professional phagocytes^{3–9} (such as epithelial cells) clear billions of apoptotic cells and particles on a daily basis^{10,11}. Since these phagocytes reside in proximity in most tissues, whether cross-communication exists between them during cell clearance, and how this might impact inflammation are not known¹². Here, we show that macrophages, via the release of a soluble growth factor and microvesicles, redirect the type of particles engulfed by non-professional phagocytes and influence their inflammatory response.

Reprints and permissions information is available at www.nature.com/reprints.

Correspondence and request for materials should be addressed ravi@virginia.edu.

Author Contributions: authors are required to include a statement to specify the contributions of each co-author. The statement can be up to several sentences long, describing the tasks of individual authors referred to by their initials. See the authorship policy page for further explanation and examples.

C.Z.H. designed, performed and analyzed most of the experiments in this study with input from K.S.R. I.J.J., J.M.K., M.W.B. assisted with *in vivo* experiments. A.L.K. provided phosphatidylserine liposomes. S.O-G ran the RNA-seq. U.E. performed microvesicle quantification using qNano. Y.M.S. performed airway resistance experiments. K.S.T. assisted in evaluation of lung pathology. C.Z.H. and K.S.R. wrote the manuscript with input from co-authors.

The authors declare no competing financial interests.

During apoptotic cell engulfment or in response to inflammation-associated cytokines, macrophages released insulin-like growth factor 1 (IGF-1). The binding of IGF-1 to its receptor on non-professional phagocytes redirected their phagocytosis, such that uptake of larger apoptotic cells was dampened while engulfment of microvesicles was enhanced. Macrophages were refractory to this IGF-1 mediated engulfment modulation. Macrophages also released microvesicles, whose uptake by epithelial cells, enhanced by IGF-1, led to decreased inflammatory responses by epithelial cells. Consistent with these observations, deletion of IGF-1 receptor in airway epithelial cells led to exacerbated lung inflammation after allergen exposure. These genetic and functional studies reveal a novel IGF-1 and microvesicle-dependent communication between macrophages and epithelial cells that can critically influence the magnitude of tissue inflammation *in vivo*.

To address potential cross-regulation among phagocytes, we initially tested a panel of eleven soluble mediators that have been linked to tissue repair, inflammation dampening, and tissue morphogenesis¹³, for their ability to modulate engulfment by LR73 fibroblasts, a non-professional phagocytic cell line. Of the eleven factors tested, only insulin-like growth factor 1 (IGF-1) significantly dampened apoptotic cell uptake, at concentrations reported in mouse and human serum (100–600 ng/mL)¹⁴ (Fig. 1a, 1b). Other factors such as EGF, FGF2, VEGF, PDGF-AA and PDGF-BB did not alter engulfment even over a range of concentrations (*Extended Data Fig. 1a*), although they all elicited early downstream signaling events (*Extended Data Fig. 1b–e*). The engulfment dampening effect of IGF-1 was also seen with airway epithelial cell lines BEAS-2B and 16HBE14o-, and the endothelial cell line SVEC-40 (Fig. 1c, *Extended Data Fig. 1f, g*).

The IGF-1 effect was not due to masking phosphatidylserine (PtdSer) on the apoptotic cells (Fig. 1d). LR73 cells express the IGF-1 receptor (IGF-1R) and IGF-1 treatment elicited phosphorylation of Akt, a signaling molecule downstream of IGF-1R (Fig. 1b). In blood, IGF-1 is bound to IGF binding proteins (IGFBPs) that stabilize and sequester IGF-1¹⁵. Addition of IGFBP3 with IGF-1 restored the phagocytic capability of LR73 cells (Fig. 1e), suggesting that binding of active IGF-1 to IGF-1R was necessary. A neutralizing antibody against the human IGF-1R reversed the engulfment-dampening effect of IGF-1 on BEAS-2B cells (Fig. 1f). Further, OSI-906 (a small molecule kinase inhibitor of IGF-1R currently tested in clinical trials¹⁶), and another inhibitor, NVP-AEW541, rescued the engulfment capacity of LR73 cells treated with IGF-1, with concomitant decrease in phosphorylation of IGF-1R and Erk (Fig. 1g and *Extended Data Fig. 2a*)¹⁷. IGF-II and insulin, which share structural similarity with IGF-1 but have lower affinities to IGF-1R¹⁸, could also reduce apoptotic cell uptake (*Extended Data Fig. 4*), albeit at higher concentrations. Thus, productive signaling through the IGF-1R is necessary for IGF-1 to dampen apoptotic cell uptake.

In contrast to the inhibitory effect on apoptotic cell uptake, IGF-1 enhanced the uptake of PtdSer containing liposomes of 150–200nm in size (Fig. 1h). This was not seen with EGF or VEGF. IGF-1 enhancement required IGF-1R signaling, as the inhibitor OSI-906 reduced the increased liposome uptake (Fig. 1h and *1i*). Thus, IGF-1 can redirect phagocytosis by non-

professional phagocytes, suppressing uptake of larger apoptotic cells while enhancing internalization of smaller particles.

The IGF-1 effect was reversible, as washing phagocytes pre-treated with IGF-1 resulted in near complete restoration of engulfment (Fig. 1j). The effect of IGF-1 on phagocytes was also rapid, as adding IGF-1 simultaneously with apoptotic cells inhibited engulfment similar to pre-treated cells (data not shown), suggesting interference at early step(s) during phagocytosis. Blocking some early signaling pathways downstream of IGF-1R, such as Akt, mTOR, Erk or PI3-kinase¹⁹, did not rescue of the IGF-1 effect (*Extended Data Fig. 3a–d*). Although IGF-1 can activate RhoA, which is known to dampen apoptotic cell engulfment²⁰, inhibiting RhoA-mediated signaling did not reverse IGF-1-mediated engulfment suppression (*Extended Data Fig. 3e,f*). Overexpressing activated Rac1 (which promotes apoptotic cell engulfment^{21,22}) bypassed attenuation of apoptotic cell uptake (Fig. 1k), suggesting that IGF-1R acts at or before a step regulated by active Rac1. Since apoptotic cell uptake requires both Rac1-dependent actin polymerization and de-polymerization²³, we explored actin regulation via IGF-1. Cytochalasin D (cytoD) that promotes actin depolymerization²⁴. Phagocytosis of apoptotic cells was potently inhibited by cytoD⁴ (data not shown). While cytoD did not affect the basal uptake of liposomes by LR73 cells, it blocked the IGF-1 induced increase in liposome uptake (Fig. 1l). Of note, cytoD treated LR73 cells appeared morphologically normal for the duration of the assay. Latrunculin A, which promotes actin depolymerization via a different mechanism²⁵, also reversed IGF-1 mediated enhancement of liposome uptake, without affecting the basal uptake of liposomes (Fig. 1m). Additionally, Arp2/3 complex can regulate phagocytosis through the formation of branched actin networks; however, CK-666, a small molecule inhibitor of Arp2/3²⁶, had minimal effect on the IGF-1 mediated increase of liposome uptake (*Extended Data Fig. 3g*). Collectively, IGF-1 mediated modulation of phagocytosis involves rapid and reversible modification of F-actin/G-actin dynamics, but likely not Arp2/3 mediated functions.

We next tested the effect of IGF-1 on professional phagocytes. Adding IGF-1 to the macrophage cell lines J774 or IC-21, or primary macrophages (bone marrow-derived or resident peritoneal macrophages), did not affect corpse uptake, even with supra-physiological concentrations of IGF-1, at every time point analyzed (Fig. 1n–p, and *Extended Data Fig. 4a, d*). Peritoneal macrophages exposed to IGF-1 also had comparable liposome uptake as control treated cells (Fig. 1q). Importantly, IGF-1R expression was confirmed in all macrophage cell types analyzed (*Extended Data Fig. 4b*) and IGF-1 initiated early signaling in macrophages, as assessed by IGF-1R and Akt phosphorylation (Fig. 1n, *Extended Data Fig. 4a*). These data suggest that IGF-1 mediated modulation of phagocytosis does not extend to macrophages.

High levels of serum IGF-1 is linked to IGF-1 production in the liver, but macrophages can also produce IGF-1 in response to the cytokine IL-4^{27,28}, raising the possibility that within a tissue, IGF-1 release from macrophages could regulate nearby non-professional phagocytes. We first confirmed IGF-1 secretion by peritoneal macrophages treated with IL-4 (Fig. 2a). Furthermore, resident peritoneal macrophages exposed to apoptotic Jurkat cells (but not live cells) produced IGF-1 (Fig. 2a). IGF-1 protein induction appears to be from newly

transcribed *Igf1* message (*Extended Data Fig. 5a*). Macrophage-produced IGF-1 could also suppress apoptotic cell uptake by LR73 cells, reversed by IGFBP3 addition (*Fig. 2b*).

To test the communication between phagocytes *in vivo*, we chose the lung, as alveolar macrophages and airway epithelial cells reside in close proximity, and both engulf apoptotic cells⁴. Alveolar macrophages, similar to the resident peritoneal macrophages, are derived from fetal monocytes²⁹, and are readily isolated via CD11c⁺ Siglec F⁺ expression, while the airway epithelial cells can be isolated and tracked via available genetic tools³⁰. IGF-1R expression was prominent in the airway epithelial cells (*Extended Data Fig. 5b*) but was also detectable at lower levels in alveolar macrophages. To test the effect of IGF-1 *in vivo*, we used mice where airway epithelial cells are specifically marked by YFP. When either apoptotic cells or liposomes were administered intranasally with IGF-1 (*Fig. 2c*), YFP⁺ airway epithelial cells had decreased apoptotic cell engulfment, but enhanced liposome uptake (*Fig. 2d, e*). Importantly, lung macrophages from the same IGF-1 treated mice were unaffected in their ability to engulf these targets (*Fig. 2d, e*). Thus, IGF-1 can differentially affect engulfment by professional and non-professional phagocytes closely residing in the same tissue.

We next tested IGF-1 release by alveolar macrophages *in vivo*. Intranasal administration of IL-4 or apoptotic Jurkat cells resulted in an increased level of IGF-1 in the bronchoalveolar lavage (BAL) fluid (*Fig. 2f*). When we tested IL-13 or IL-5 (cytokines linked to lung homeostasis and inflammation³¹), IL-13 (whose receptor shares a common subunit with the IL-4R³²), but not IL-5, induced IGF-1 production (*Fig. 2f*). Since the source of IGF-1 is difficult to distinguish in these experiments, we generated LysM-Cre/*Igf1^{fl/fl}* mice^{33,34}, targeting IGF-1 deletion in the myeloid lineage. LysM-Cre/*Igf1^{fl/fl}* mice showed loss of *Igf1* mRNA in alveolar macrophages (*Extended Data Fig. 5c*) and IGF-1 induction after IL-4, IL-13 or apoptotic cell treatment (*Fig. 2H*). This suggested the macrophage/myeloid population as the predominant source of inducible IGF-1 in the lung.

To investigate IGF-1/IGF-1R signaling in inflammation, we used a model of airway inflammation induced by the allergen house dust mite (HDM), where apoptotic cell recognition by airway epithelial cells influences inflammation^{4,35}. We administered HDM intranasally in the allergen sensitization and challenge stage, modeling the natural route of allergen encounter (*Fig. 3a*). When we first tested LysM-Cre/*Igf1^{fl/fl}* mice, these mice proved unsuitable, as we continued to detect variable levels of IGF-1 in the BAL fluid after HDM administration (likely due to leakage of serum IGF-1 during inflammation). Therefore, we targeted instead the IGF-1R on the epithelial cells. We crossed *Igf1R^{fl/fl}* mice³⁶ with CCSP- τ TA/tetO-Cre transgenic mice^{30,37}, the latter driving Cre under the Club cell secretory protein (CCSP) promoter in the epithelial cells of the trachea, bronchi and bronchioles^{30,37}. This CCSP- τ TA/tetO-Cre strain allows for inducible Cre expression through doxycycline administration via drinking water, thereby allowing normal development and gene deletion just prior to allergen exposure. We observed near complete loss of IGF-1R on epithelial cells of CCSP-Cre/*Igf1R^{fl/fl}* mice after doxycycline treatment (*Fig. 3b*). After sensitization and challenge with low-endotoxin HDM, the CCSP-Cre/*Igf1R^{fl/fl}* mice had greater airway inflammation based on several parameters. First, there was marked increase in eosinophils and CD4⁺ T-cells in the BAL fluid (*Fig. 3c*) and trending increase in

inflammatory cells in lungs (*Extended Data Fig. 6a*). Second, lung-draining lymph nodes were larger with more CD4⁺ T-cells (*Fig. 3d*). Third, lung sections showed increased peribronchial and perivascular cellular infiltration (*Fig. 3e, f*) and greater mucus accumulation after HDM treatment (*Fig. 3g, h*). Fourth, HDM-treated CCSP-Cre/*Igf1r^{fl/fl}* mice displayed increased airway reactivity after methacholine challenge, a measure of the bronchial hyper-responsiveness^{38,39} (*Extended Data Fig. 6b*). There were more apoptotic cells in lung sections (cleaved caspase 3 staining), likely due to greater inflammation (*Extended Data Fig. 6c*). These data suggested a requirement for IGF-1R in the airway epithelial cells in minimizing inflammation in this model.

These observations were initially surprising, as we were expecting the loss of IGF-1R on airway epithelial cells to improve apoptotic cell clearance and thereby attenuate, rather than worsen, inflammation. This prompted us to examine the temporal requirement of IGF-1/IGF-1R signaling in epithelial cells during allergen exposure. To distinguish the requirement for IGF-1/IGF-1R signaling at the sensitization versus challenge phase, we administered doxycycline at different times: deleting IGF-1R expression *before* allergen sensitization (*Fig. 4a*), or *after* the initial allergen sensitization but before the allergen challenge phase (*Extended Data Fig. 7a*). Mice with IGF-1R deletion prior to allergen sensitization showed a significant increase in inflammatory parameters (*Fig. 4b*), while deleting IGF-1R after the sensitization phase had minimal effect on disease severity (*Extended Data Fig. 7b, c*).

Airway epithelial cells encountering allergen can produce cytokines, such as TSLP, CSF-2/GM-CSF (affecting dendritic cell maturation), as well as IL-33 and IL-25 that drive type 2 innate lymphoid cells (ILC2s) to proliferate and produce IL-13⁴⁰. Bronchial epithelial cells from human asthmatics produce elevated levels of IL-6, IL-8, and CSF-2⁴¹, and TSLP released from airway epithelial cells (mice and human) can exacerbate airway inflammation⁴². When we assessed the cytokine profile in the BAL fluid of CCSP-Cre/*Igf1r^{fl/fl}* mice sensitized with HDM, levels of IL-6 and TSLP were greater (*Fig. 4d, e*). We did not find increased levels of IL-33, as seen with Rac1 deletion in airway epithelial cells⁴, but this may be due to differences in inflammatory pathways regulated by the loss of IGF-1R versus Rac1. These results suggest that IGF-1R in airway epithelial cells limits inflammatory cytokines during the initial antigen exposure/sensitization phase.

As for trigger(s) for IGF-1 release from the alveolar macrophages in the sensitization phase, while IL-4 is often considered a classic Th2 cytokine from the adaptive immune response^{43,44}, both IL-4⁴⁵⁻⁵¹ and IL-13⁴⁰ can be produced during the allergen sensitization phase by resident mast cells, basophils, and/or ILC2s. In fact, IL-4 was enhanced (along with IL-5 and eotaxin-1) in the BAL fluid of CCSP-Cre/*Igf1r^{fl/fl}* mice sensitized with HDM (*Fig. 4c*). Thus, IL-4 and/or apoptotic cells present during the initial allergen exposure could elicit IGF-1 production from alveolar macrophages.

Alveolar macrophages are reported to release microvesicles containing anti-inflammatory mediators during smoking-induced lung injury⁵². Since IGF-1 enhances liposome uptake by airway epithelial cells, we tested whether microvesicles from alveolar macrophages may impact airway epithelial cell response to HDM. Using differential centrifugation and filtration, we isolated and characterized microvesicles from alveolar macrophages (*Fig. 4f*).

First, negative stain and cryo-electron microscopy revealed membrane bound spherical structures >100nm in diameter (Fig. 4g, h). Second, via *ImageStreamXTM* analysis, particles from an alveolar macrophage cell line or primary mouse alveolar macrophages carry markers of lung macrophage origin, CD11c or SiglecF, with variable Annexin V staining (Fig. 4i). Third, tunable resistive pulse sensing analysis of microvesicles revealed a mean particle size of 357 ± 148.5 nm (Fig. 4j), within the reported 100–1000nm range for microvesicles⁵³. Further, IL-4 treatment of macrophages increased microvesicles secretion (*Extended Data Fig. 8a*). Also, uptake of these microvesicles by BEAS-2B airway epithelial cells was enhanced by IGF-1 (Fig. 4k). Importantly, adding alveolar macrophage derived microvesicles to HDM-treated BEAS-2B cells resulted in significantly lower *TSLP*, *CSF2*, *IL6*, and *IL8* induction (Fig. 4l). To further explore this, we performed RNA-seq of BEAS-2B cells treated with HDM \pm microvesicles. While HDM treatment increased several known genes associated with asthma in humans^{54–57}, such as FGF2, KLF4, Interferon-Induced Protein with Tetratricopeptide Repeats 2 (IFIT2), and Pentraxin 3 (PTX3), adding microvesicles from alveolar macrophages suppressed transcription of these genes in the epithelial cells (Fig. 4m, *Extended Data Fig. 8b*). Thus, microvesicles released from alveolar macrophages acting on airway epithelial cells exposed to allergen could dampen airway inflammation.

The data presented here provide several new insights on phagocytosis and tissue inflammation. First, it has long been known that professional and non-professional phagocytes reside in proximity and can engulf dying cells and debris, yet communication between these phagocytes was not understood. The data presented here identifies a rapid, transient, and reversible regulation, wherein soluble IGF-1 from macrophages influences the type of particle uptake by epithelial cells. This transient effect might allow the macrophages to temporarily ‘redirect’ the non-professional phagocytes toward other function(s). Such a possible hierarchy in cell clearance could provide temporal and spatial cross-communication within a given tissue¹⁰. Second, our data identifies a two-part regulation of epithelial cells by macrophages which impacts airway inflammation, i.e., the secretion of IGF-1 that redirects particle uptake, and the release of microvesicles that dampen inflammatory cytokine production by epithelial cells (*Extended Data Fig. 9*). Third, IGF-1 is a growth factor widely linked to growth, cellular proliferation, and aging^{58–61}. Global IGF-1 deletion in mice results in dwarfism and perinatal lethality, and IGF-1 mutations are linked to human diseases^{34,62,63}. This work identifies a previously unappreciated biological function for the IGF-1/IGF-1R axis as a modulator of airway hyper-responsiveness to allergens with potential therapeutic relevance.

Methods

Mice

C57BL/6J, *Igf1^{fl/fl}*, and *Igf1^{fl/fl}* mice were obtained from Jackson Laboratories. CCSP-rtTA/tetO-Cre were kindly provided by Dr. Jeffrey Whitsett at Cincinnati Children’s Hospital³⁷. To generate IGF-1R deletion in Club cells, we crossed CCSP-rtTA/tetO-Cre mice to *Igf1^{fl/flB6}*. To achieve deletion, mice were given doxycycline (1mg/mL) in drinking water containing 0.4% sucrose for at least 7 days prior to beginning of allergen administration,

unless otherwise noted. We also crossed *Igfl^{fl/fl}* mice^{33,34} to LysM-Cre mice to conditionally delete *Igfl* in the myeloid lineage. We have previously reported on the generation of CCSP-Cre/YFP mice⁴. For all *in vivo* experiments, except generation of apoptotic thymocytes, mice between the ages of 8 and 12 weeks were used. No blinding was performed for *in vivo* experiments. Mice were allocated to experimental groups based on genotype and age-matching. Female and male mice were used for all experiments, except for *in vivo* engulfment assays in which only male mice were used. Sample size was selected based on mice availability and power statistics. All animal procedures were performed according to the protocols provided by the Institutional Animal Care and Use Committee (IACUC) of the University of Virginia.

Induction of Airway Inflammation

Mice were given drinking water containing doxycycline (1mg/mL) seven days prior to first HDM administration. Mice were primed intranasally with 10 μ g of low endotoxin house dust mite extraction (Indoor Biotechnologies) on days 0, 2, 4 and then challenged intranasally on days 10, 12, and 14. On day 16, mice were harvested and analyzed for eosinophilic airway inflammation. Alternatively, mice were given three doses of low endotoxin HDM on days 0, 2, and 4 and analyzed on day 6 (“sensitization phase”). For the “challenge phase,” mice that had not received any doxycycline were given three doses of low endotoxin HDM on days 0, 2 and 4, then given doxycycline (via drinking water) from day 4 until the mice were analyzed. These mice were also challenged intranasally with three doses of low endotoxin HDM on days 10, 12, and 14 and analyzed on day 16. For airway inflammation experiments, sample size was selected to be above 3 mice per group per experiment.

Collection of BAL fluid, lymph nodes, and lung

For airway inflammation experiments, 0.8mL of PBS were delivered intratracheally through a cannula. Recovered BAL fluid was centrifuged and the supernatant was frozen at -80°C for subsequent Luminex analysis. Collected cells were stained for surface markers to distinguish macrophages, neutrophils, T-cells, and eosinophils. For lung harvests, mice were perfused through the right ventricle with PBS and the lungs were carefully excised and placed in type 2 collagenase (Worthington Biochemical Corporation) dissolved in HBSS containing Ca^{2+} and Mg^{2+} . Lungs were minced and then incubated at 37°C for one hour, with vigorous pipetting to separate the tissue every 15 minutes. The lung homogenate was then passed through a 70 μm nylon strainer, spun down and treated with red blood cell lysis buffer (Sigma-Aldrich) for 5 minutes. The cells were then washed and resuspended in PBS containing 0.1% BSA. Draining lymph nodes were carefully extracted, and a single cell suspension was made by passage through a 70 μm nylon strainer using the flat end of a syringe. Cells were washed and then resuspended in PBS containing 0.1% BSA.

Cell staining and total cell numbers

The collected cells were stained for macrophages, neutrophils, T cells, and eosinophils using the following markers: CD11c (eBioscience, cl. N418), Siglec F (BD Biosciences, cl. E50-2440), Ly6G (eBioscience, clone 1A8), CD11b (eBioscience, cl. M1/70), F4/80 (eBioscience, cl. BM8), CD3 (eBioscience, cl. 145-2C11), CD4 (eBioscience, cl. RM4-5), CD44 (eBioscience, cl. IM7), CD69 (eBioscience, cl. H1.2F3). Absolute cell numbers were

determined using AccuCount Particles (Spherotech). Flow cytometry data was collected on FACS Canto I (Becton Dickinson) and analyzed with FlowJo (Treestar, Inc).

Microscopy and histology

For hematoxylin and eosin and Periodic acid Schiff staining of lung sections, mice were perfused with PBS and a cannula inserted into the trachea. The lungs were gently inflated with 10% formalin at a constant fluid pressure at 25 cm. The trachea was tied off and the entire heart and lung were removed and placed in 10% formalin. Lungs were paraffin embedded, sectioned and stained by HistoTox Labs (Boulder, CO). Additional lung sections were embedded and sectioned by Research Histology Core at University of Virginia and the immunohistochemical staining for IGF-1R, and cleaved caspase 3 was performed by the University of Virginia Biorepository and Tissue Research Facility. Approximately 6–10 images were taken per mice, with a total of 3–4 mice per group, and blindly scored by two independent scorers for inflammation, PAS staining, and cleaved caspase 3 positive cells. Immunofluorescence staining of lung sections was performed at the University of Virginia Cardiovascular Research Center Histological Services.

Airway hypersensitivity

Mice were anesthetized and given a tracheotomy tube that delivered increasing concentrations of aerosolized methacholine. The tracheotomy tube in turn was connected to the inspiratory and expiratory ports of a volume-cycled ventilator (flexiVent; SCIREQ Scientific). Airway resistance was measured at baseline and after each dose of methacholine.

Macrophage isolation

To obtain bone-marrow derived macrophages, femurs were removed from 8 week old mice and flushed with 5mL of sterile PBS containing 5% FBS. The cell suspension was centrifuged, treated with red blood cell lysis buffer, washed, and then plated onto sterile petri dishes in DMEM containing 10% L929 media, 10% FBS and 1% penicillin/streptomycin/ glutamine (PSQ). Media was replenished every 2 to 3 days and differentiated cells were used at day 6 post-harvest. Resident peritoneal macrophages were obtained by flushing the peritoneal cavity of mice with 10mL of cold PBS containing 5% FBS. Collected cells were spun down, resuspended in X-VIVO 10 (Lonza) and plated at a concentration of 3×10^5 cells per well in a 24 well plate for IGF-1 secretion assays, and 5×10^5 per well in a 24 well plate for engulfment assays. Floating cells were washed the next day and remaining peritoneal macrophages were used 2 days after isolation. Alveolar macrophages were isolated by flushing the lungs with 1mL of cold PBS instilled intratracheally (five flushes). Collected cells were centrifuged, resuspended in F12K media containing 10% FBS and 1% PSQ, and seeded at 1×10^5 cells per well in a 48-well plate. All floating cells were washed away the next day and remaining cells were used in assays 2 days after isolation.

Microvesicle isolation

MH-S, mouse alveolar macrophages, or primary mouse alveolar macrophages were seeded. After adherence, the media was replaced with .22 μ m filtered media to remove any contaminating microvesicles. After an overnight incubation, the supernatant was harvested

and spun at 5000xg to remove cell debris and apoptotic bodies. The pellet was discarded and the resulting supernatant was filtered through 0.8µm filter and spun again at 17,000xg. The pelleted microvesicles were then washed with HBSS and then spun again at 17,000xg. For engulfment assays, microvesicles were stained with TAMRA for 20 minutes and then added to BEAS-2B cells for 90 minutes. For flow cytometry, purified particles were stained with CD11c, Siglec F, and Annexin V (BD Biosciences, Cat. No. 550475) and processed on ImagestreamX™ imaging flow cytometer (Amnis). Microvesicle size distribution was characterized using qNano (IZON Science) with a NP400 membrane and at least 500 particles were counted. Microvesicles were prepared for cryo-electron microscopy using standard methods and imaged on an FEI TF20⁶⁴.

***In vivo* cytokine or apoptotic cell administration**

Mice were administered intranasally with 1µg of recombinant mouse IL-4, IL-5, or IL-13 (eBiosciences), 1×10^6 apoptotic Jurkat cells, or PBS as control, for two consecutive days. On the third day, BAL fluid was recovered and centrifuged; the supernatant was stored at -80°C for subsequent cytokine analysis. For cytokine or apoptotic cell administration, sample size was selected to be 2 or more mice per group per experiment.

Cytokine and IGF-1 analysis

IL-4, IL-5, IL-6, and CCL-11 in the BAL fluid of mice that only received priming with HDM (regimen #1) were quantified by a multiplex Luminex performed by the University of Virginia Flow Cytometry Core Facility. Secretion of IGF-1 from J774 cells, peritoneal macrophages, and BAL fluids, as well as TSLP from BAL fluids, were measured by ELISA (R&D Systems).

***In vitro* cell systems**

LR73 (hamster fibroblasts), SVEC-40 (mouse endothelial cells), BEAS-2B (human bronchial epithelial cells, ATCC #CRL-9609), 16HBE14o- cells (human bronchial epithelial cells), MH-S (mouse alveolar macrophage cells ATCC #CRL-2019), Jurkat (human T-cells) were either available in the laboratory or obtained from ATCC, with the latter tested for mycoplasma.

***In vitro* engulfment assay**

LR73, SVEC-40, BEAS-2B, and 16HBE14o- cells were seeded in a 24 well plate. Thymocytes were isolated from 4–6 week old mice and induced to undergo apoptosis with dexamethasone. Thymocytes or prepared microvesicles were then stained with either CypHer5E (GE Healthcare, PA15401) or TAMRA (Invitrogen, C-1171). LR73 and SVEC-40 cells were incubated with apoptotic thymocytes at a 1:10 phagocyte to target ratio, BEAS-2B at a 1:5 phagocyte to target ratio, and 16HBE14o- at a 1:20 phagocyte to target ratio for 2 hours. Mouse IGF-1 (Sigma-Aldrich), human IGF-1 (Sigma-Aldrich), human IGF-II (Sigma-Aldrich) were added to the phagocytes at the same time as addition of apoptotic targets. For IGFBP3 studies, IGFBP3 (Sigma-Aldrich) was added to media or supernatant from J774 cells for one hour to allow IGFBP3 to bind to any available IGF-1, then the mix is added to phagocytes along with apoptotic targets. For all pharmacological

studies, phagocytes were pre-incubated with the compounds listed below for one hour prior to addition of apoptotic targets: cytochalasin D (Sigma-Aldrich, C8273, 1 μ M), Latrunculin A (Tocris, 3973, 150nM), CK-666 (Tocris, 3950, 25 μ M-100 μ M), OSI-906 (Selleckchem, S1091, 5nM-40nM), NVP-AEW541 (Selleckchem, S1034, 25nM-100nM), Rapamycin (Sigma-Aldrich, R0395, 10 μ M-1mM), MK-2206 2HCl (Selleckchem, S1078, 10nM-1 μ M), U0126-EtOH (Selleckchem, S1102, 8pM-5nM), Wortmannin (Sigma-Aldrich, W1628, 50nM-200nM), Y27632 (Calbiochem, 688000, 3.75 μ M-15 μ M), or GSK269962 (Tocris, 4009, 80nM-2 μ M). Phagocytes were examined to ensure no gross morphological changes occurred due to drug treatment. Targets were then washed off three times with PBS, and the cells were dissociated from the plate with trypsin and the engulfment assessed by flow cytometry.

***In vivo* engulfment assay**

CCSP-Cre/YFP mice were administered PBS or 1 μ g of IGF-1 intranasally. One hour later, 100 million CypHer5E-labelled apoptotic thymocytes with or without IGF-1 were injected intranasally for 3.5 hours. The BAL fluid was harvested and the lungs excised, minced, and digested into a single cell suspension. The cells were then stained with appropriate markers: CD11c and Siglec F for alveolar macrophage markers and EpCam (along with YFP expression) for airway epithelial cells and analyzed by flow cytometry to assess apoptotic cell uptake by the airway epithelial cells and the alveolar macrophages.

Liposome construction

Liposomes were prepared by dissolving the lipids (phosphatidylserine, dioleoyl phosphatidylcholine, cholesterol and the lipid DiD dye) in chloroform, evaporating chloroform under flow of argon gas in a glass vial, then subjecting the lipid layer to overnight lyophilization to remove traces of organic solvent. Then normal saline was added for hydration, and intense vortexing was performed to prepare multilamellar vesicles (MLV). Liposomes were repeatedly filtered through a 0.2 μ m Nuclepore polycarbonate filter to prepare smaller particles. Particle size was verified by dynamic light scattering using Nicomp 370.

Immunoblotting

LR73, J774 or BEAS-2B cells were seeded in a 60mm dish at a concentration of 5×10^5 . Cells were serum-starved for 6 hours and then stimulated with 100ng/mL of IGF-1 for various time points. Cells were lysed in RIPA buffer and used in Western blots. The blots were probed for phospho-Erk1/2 (Cell Signaling Technology, #4370), phospho-Akt (Cell Signaling Technology, #4060), phospho-IGF-1R (Cell Signaling, #3024), total Erk2 (Santa Cruz Biotechnology, #sc-154-G), total Akt (Cell Signaling Technology, #4691), total IGF-1R (Cell Signaling, #9750), and anti-B-actin-HRP (Sigma-Aldrich, #A3854) followed by chemiluminescence detection.

Quantitative RT-PCR

Total RNA was extracted from cells using Quick-RNA Miniprep Kit (Zymo Research) or RNeasy Mini Kit (Qiagen) and cDNA was synthesized using QuantiTect Reverse

Transcription Kit (Qiagen) according to manufacturers' instructions. Quantitative gene expression for mouse *Igf1*, human *TSLP*, *CSF2*, *IL6*, *IL8* or housekeeping human or mouse *Hprt* was performed using Taqman probes (Applied Biosystems) using StepOnePlus Real Time PCR System (ABI).

RNA-seq

BEAS-2B cells were treated with HDM and alveolar macrophage-derived microvesicles for 3 hours. Total RNA was extracted and an mRNA library was prepared using Illumina TruSeq platform and followed by transcriptome sequencing using an Illumina NextSeq 500 cartridge. Rv3.2.2 was used for graphical and statistical analysis and the R package DESeq2 was used for differential gene expression analysis of RNA-seq data. RNA-seq analysis was performed by the UVa Bioinformatics Core.

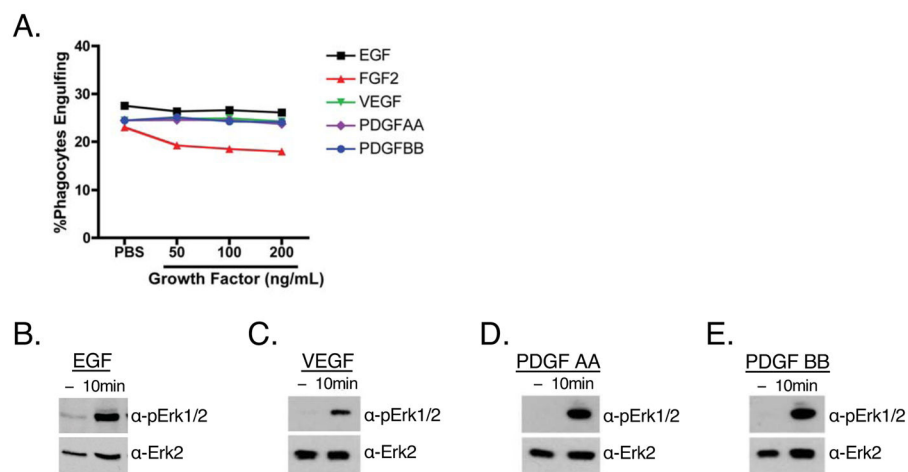
Code Availability

R code used for bioinformatics analysis and heat map generation is available upon request.

Statistical analysis

Statistical significance was determined using GraphPad Prism 5 or 6 using unpaired Student's two-tailed *t*-test, one-sample *t*-test, one-way ANOVA or two-way ANOVA, as according to test requirements. Grubbs' Outlier Test was used to determine outliers, which were excluded from final analysis. A *p*-value of <0.05 (indicated by one asterisk), <0.01 (indicated by two asterisks), or <0.001 (indicated by three asterisks) were considered significant.

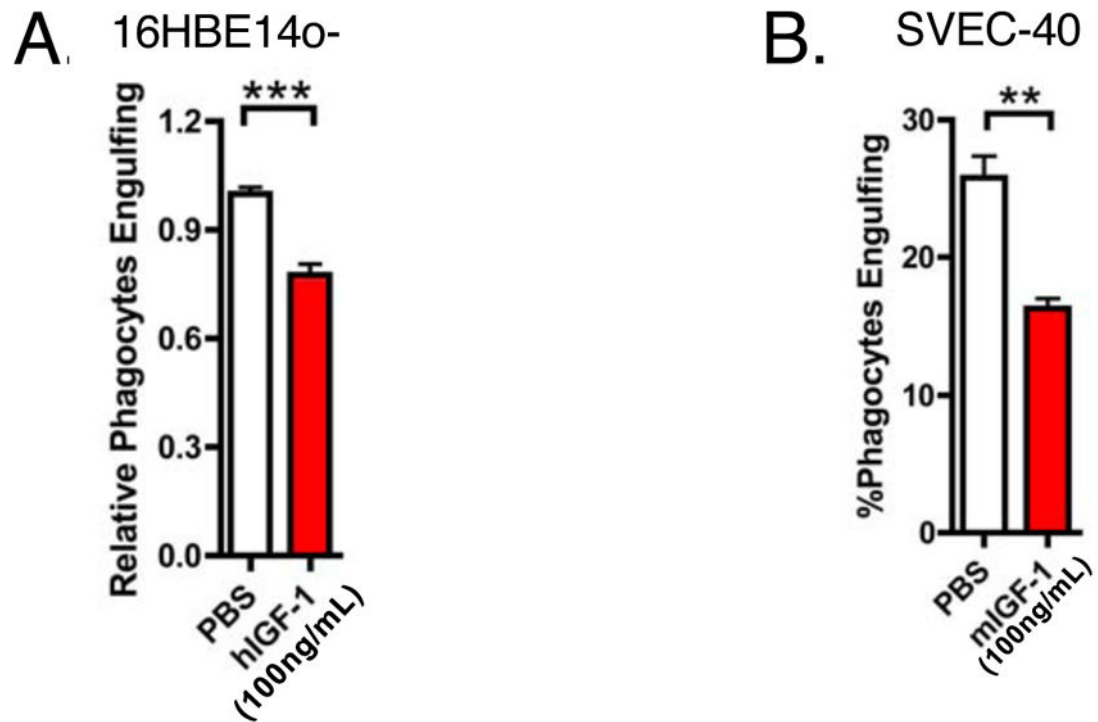
Extended Data



Extended Data Figure 1. Erk1/2 is phosphorylated in LR73 cells stimulated with EGF, VEGF, PDGF AA/BB

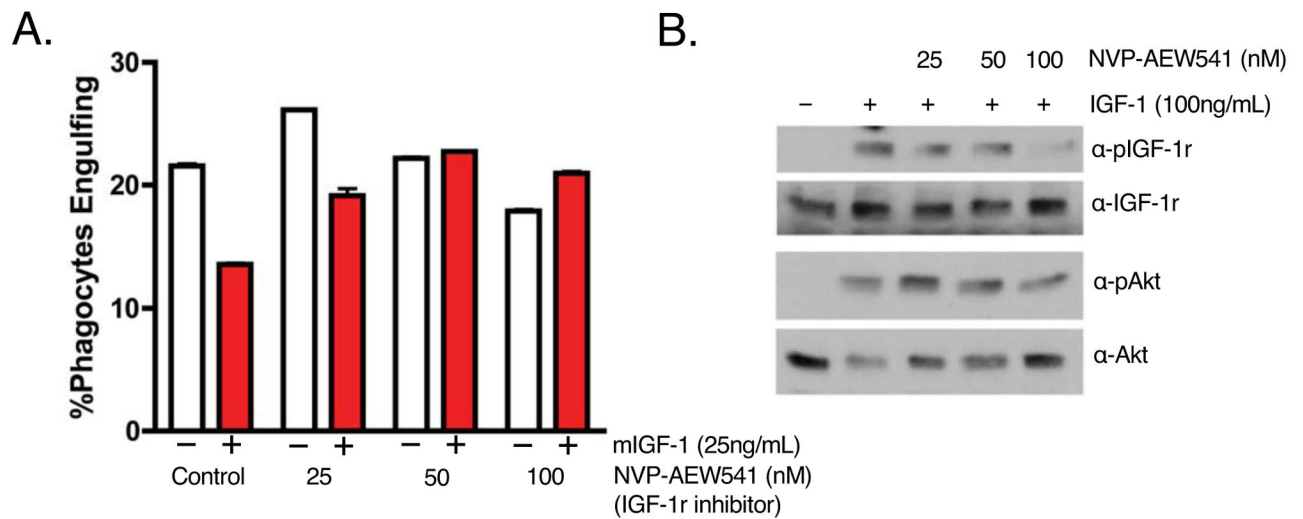
(A) Representative engulfment assay in which LR73 cells were treated with indicated growth factors at increasing concentrations and assessed for engulfment of apoptotic thymocytes ($n=3$). (B–D) Serum-starved LR73 cells were stimulated with 100ng/mL of

indicated growth factors for 10 minutes and the phosphorylation of Erk1/2 was determined by immunoblotting (n=2).



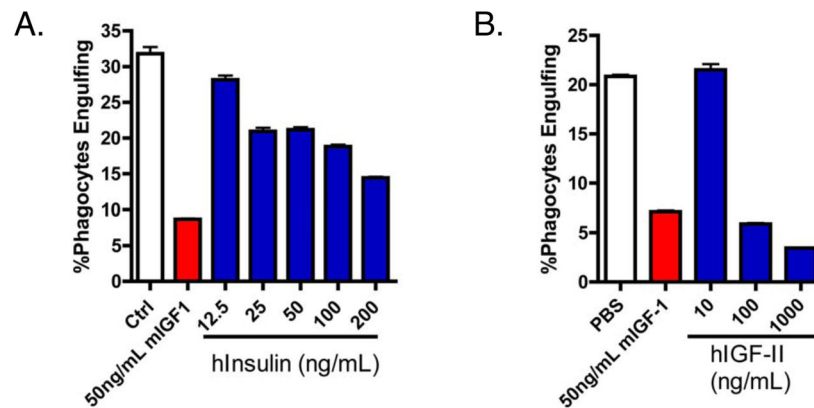
Extended Data Figure 2. 16HBE14o- cells and SVEC-40 cells engulf less apoptotic cells when exposed to IGF-1

(A) Representative engulfment assay in which the uptake of apoptotic thymocytes by 16HBE14o- human airway epithelial cells is dampened by IGF-1 treatment (n=3). (B) Engulfment of SVEC-40 endothelial cells treated with IGF-1 with apoptotic thymocytes as targets (n=3). Data represented as mean \pm s.d. A *p*-value of <0.05 (indicated by one asterisk), <0.01 (indicated by two asterisks), or <0.001 (indicated by three asterisks).



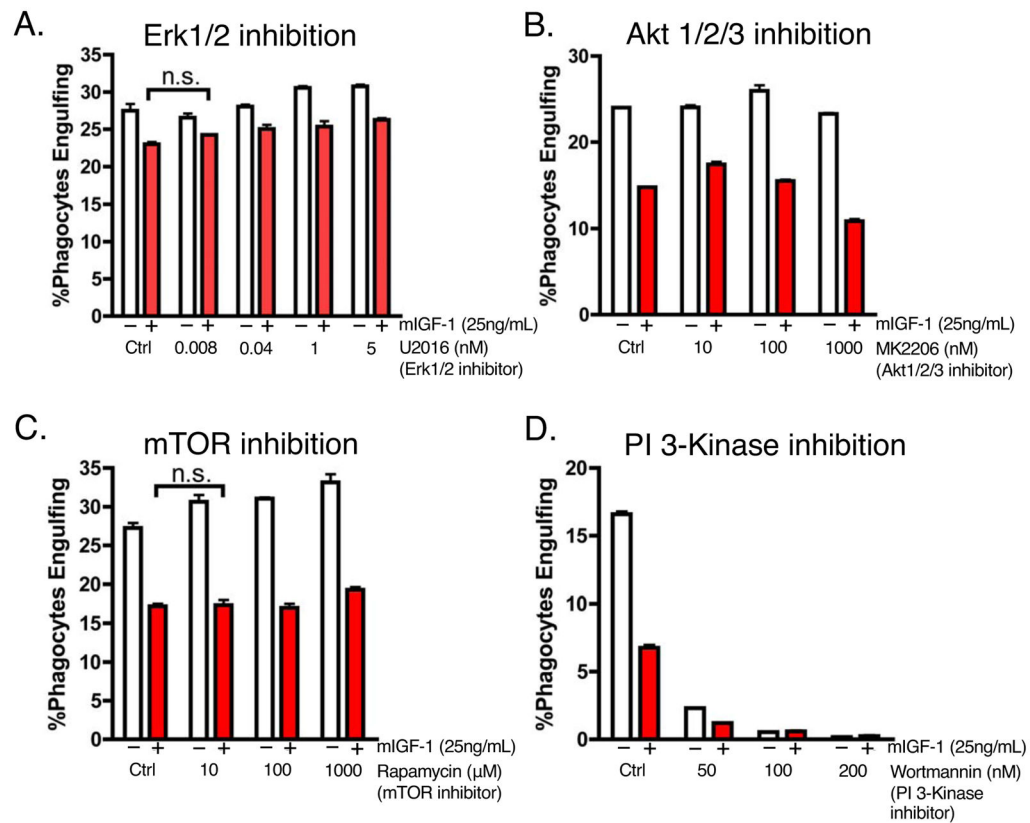
Extended Data Figure 3. A second IGF-1r inhibitor, NVP-AEW541, also reverses inhibition of apoptotic cell engulfment due to IGF-1

(A) Engulfment of apoptotic thymocytes by LR73 cells treated with various doses of NVP-AEW541, a small molecule inhibitor of IGF-1r (n=3). (B) Representative Western blot of LR73 cells stimulated with IGF-1 and treated with increasing doses of NVP-AEW541 (n=2). Data represented as mean \pm s.d.



Extended Data Figure 4. LR73 cells treated with recombinant insulin or IGF-II engulf less apoptotic cells

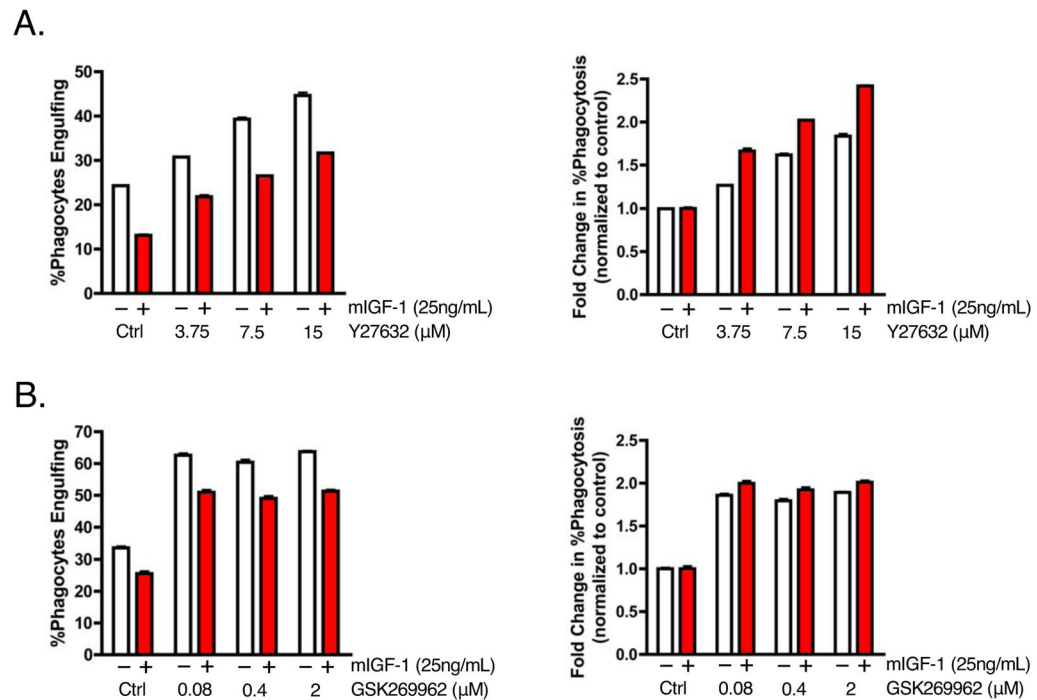
Engulfment of apoptotic thymocytes by LR73 cells that were treated with the indicated concentrations of human insulin (A) and human IGF-II (B) (n=2). Data represented as mean \pm s.d.



Extended Data Figure 5. Blocking canonical signaling intermediates downstream of IGF-1 receptor signaling does not reverse the IGF-1 mediated engulfment suppression

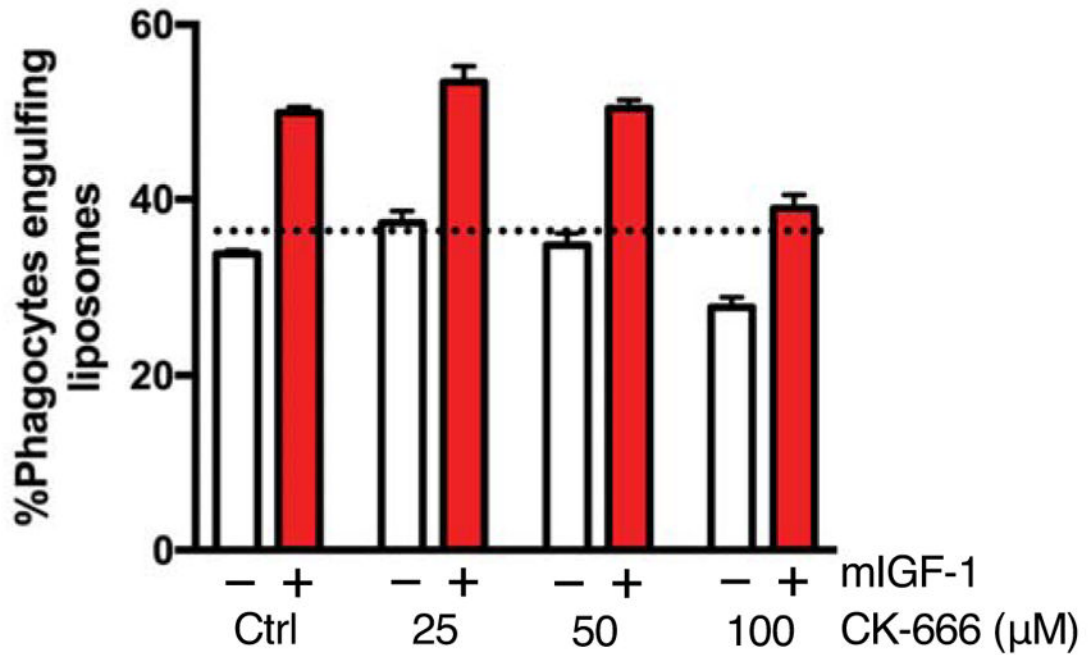
(A–D) Engulfment of apoptotic thymocytes by LR73 cells treated with U2016 (Erk1/2 inhibitor) (A), MK-2206 (Akt1/2/3 inhibitor) (B), Rapamycin (mTOR inhibitor) (C), or Wortmannin (PI 3-Kinase inhibitor) (D) in the presence or absence of IGF-1 (n=2–3).

Wortmannin has been previously demonstrated to inhibit phagocytosis of apoptotic cells and adding IGF-1 does not alter this inhibition. Data represented as mean \pm s.d.



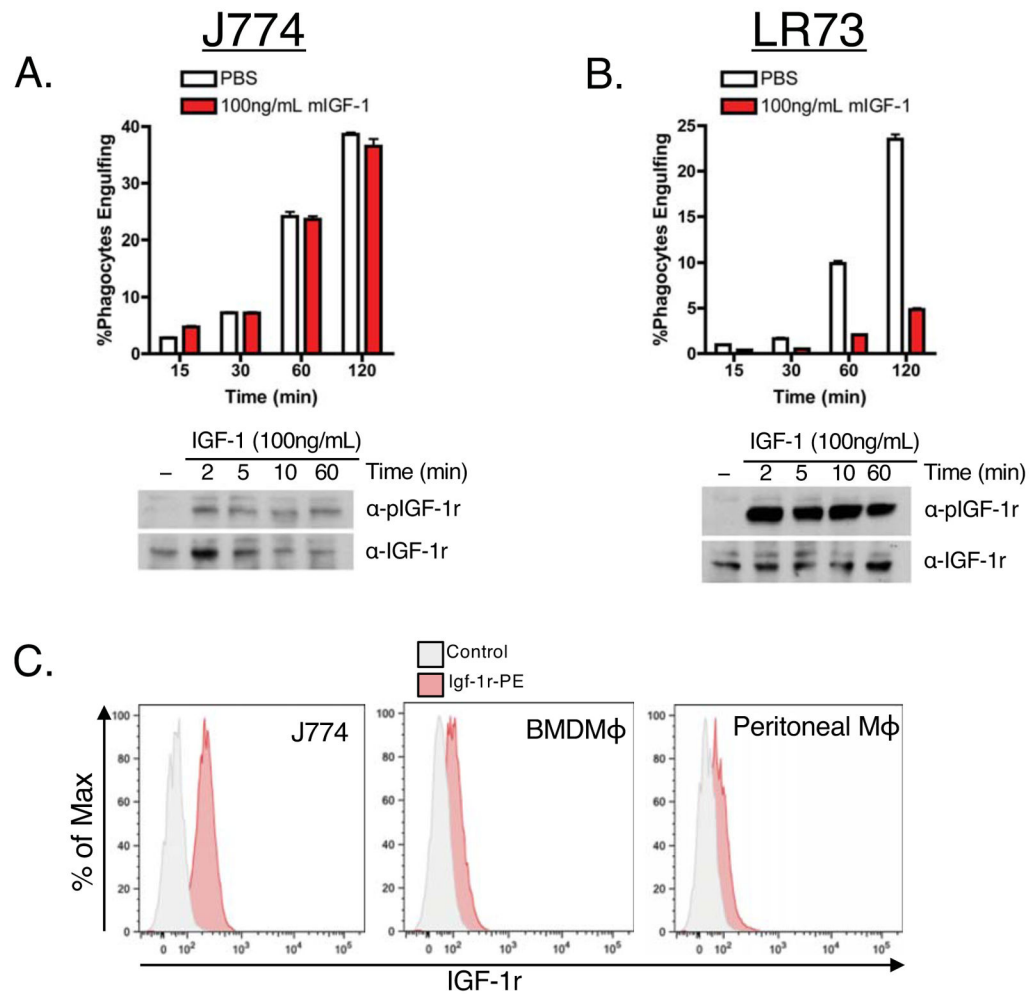
Extended Data Figure 6. Inhibition of Rho-kinase (ROCK) does not appear to rescue IGF-1 induced engulfment suppression in LR73 cells

(A–B) (Left panel) Engulfment assay of LR73 cells treated with various doses of either Rho kinase inhibitors Y27632 or GSK269962 in the presence or absence of IGF-1 ($n=2-3$). Initially, it appeared that inhibition of ROCK was able to partially rescue IGF-1 induced engulfment suppression. However, as ROCK inhibition basically increases phagocytosis of apoptotic cells (consistent with what has been previously reported), we normalized the change in phagocytosis for each inhibitor concentration to the appropriate control (right panel). After normalizing, we observed that ROCK inhibition did not increase corpse uptake in LR73 cells in the presence of IGF-1 more than the increase observed basally due to Rho kinase inhibition. Thus, inhibition of ROCK does not appear to rescue IGF-1 induced engulfment suppression. Data represented as mean \pm s.d.



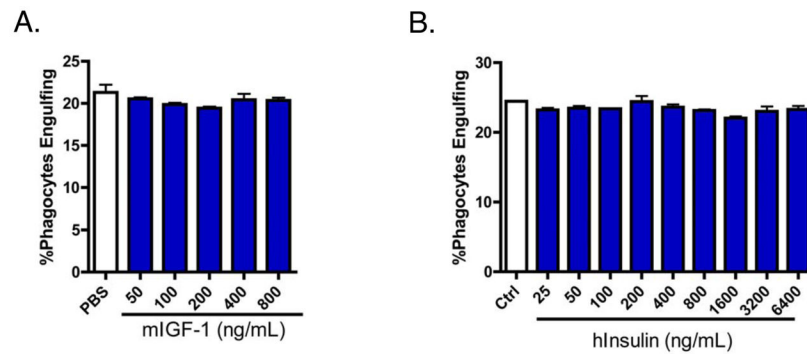
Extended Data Figure 7. Inhibition of Arp2/3 mediated functions does not appear to reverse IGF-1 mediated enhancement of liposome uptake

LR73 cells were treated with CK-666 at the concentrations indicated and then assessed for uptake of liposomes in the presence of IGF-1 (n=3). Data are represented as mean \pm s.d.



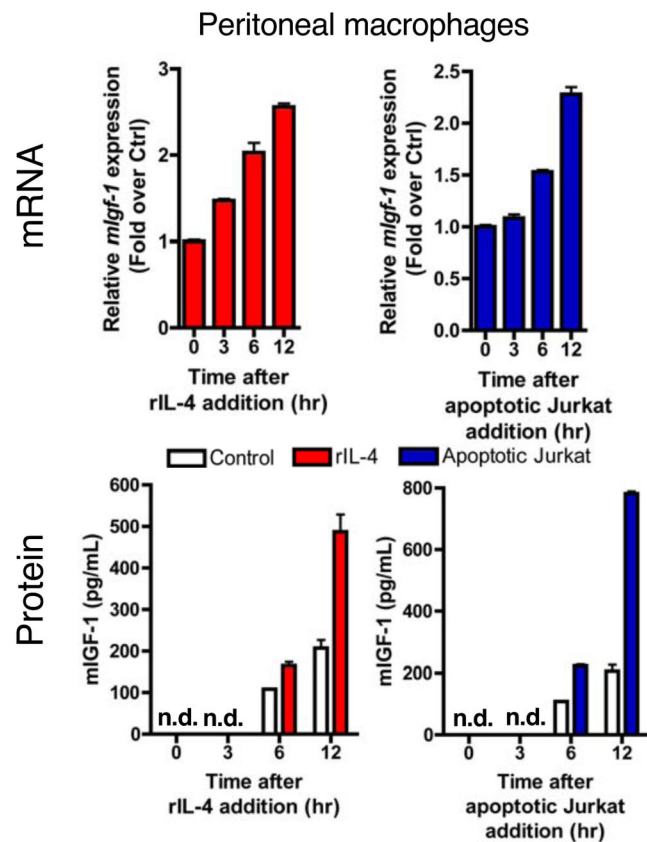
Extended Data Figure 8. J774 and LR73 cells phosphorylate IGF-1r upon IGF-1 stimulation similarly

J774 cells (A) or LR73 cells (B) treated with 100ng/mL mouse IGF-1 treated were assess for their ability to engulf apoptotic thymocytes (upper) or serum-starved for 6 hours and stimulated with 100ng/mL mouse IGF-1 and assessed for phosphorylation of IGF-1R by Western blot (bottom). (C) Flow cytometry histograms of IGF-1r expression on J774 cells (left), BMDMφ (middle), and peritoneal macrophages (right) (n=3–4). Data represented as mean ± s.d.



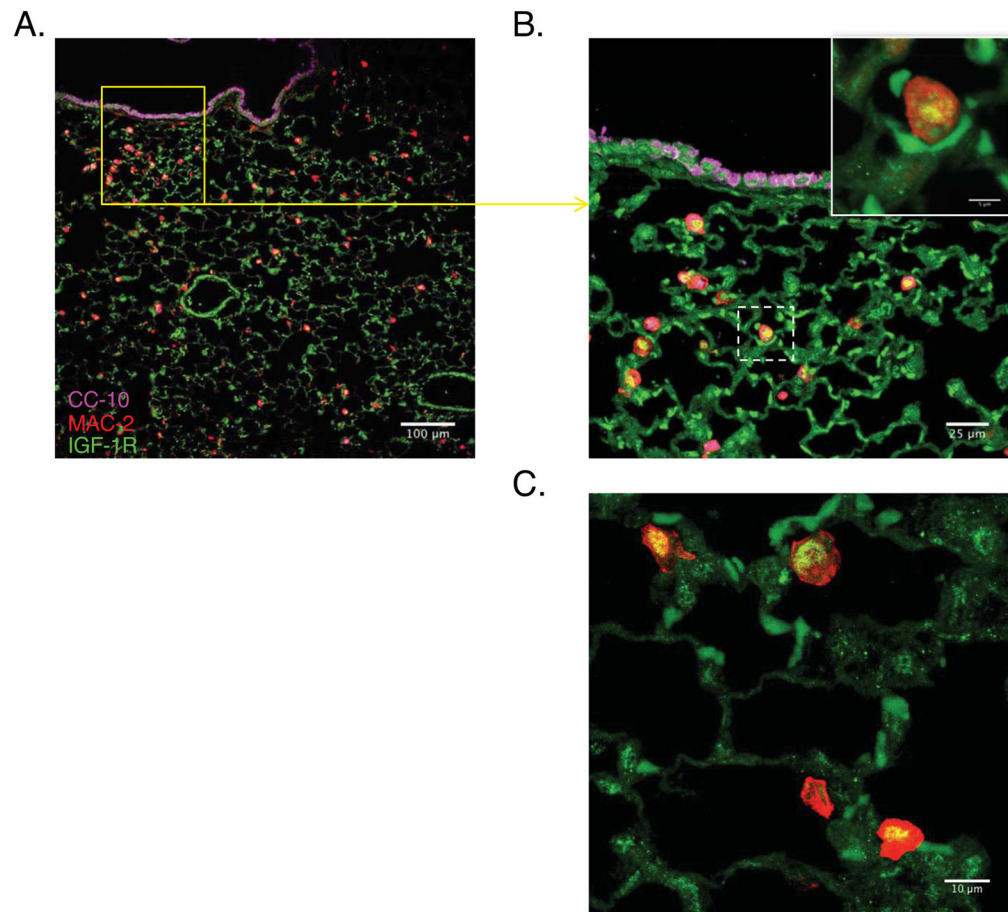
Extended Data Figure 9. IGF-1 and insulin do not modulate apoptotic cell uptake in the IC-21 macrophage cell line

IC-21 cells treated with indicated concentrations of mouse IGF-1 (**A**) and human insulin (**B**) were assessed for their ability to engulf apoptotic thymocytes (n=2–3). Data represented as mean \pm s.d.



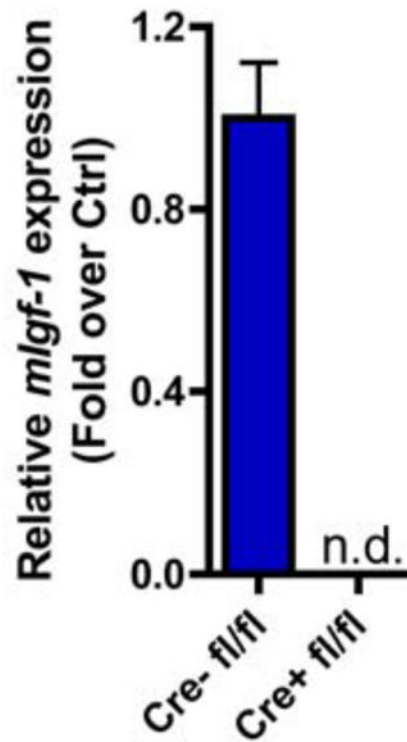
Extended Data Figure 10. Production of IGF-1 by peritoneal macrophages after apoptotic cell or IL-4 stimulation is mostly likely new transcription

Peritoneal macrophages were either untreated, stimulated with rIL-4 or apoptotic Jurkat cells and *Igf1* mRNA (top panels) and IGF-1 protein in the supernatant (bottom panels) were assessed in a time course (n.d. refers to not detected) (n=3). Data represented as mean \pm s.d.



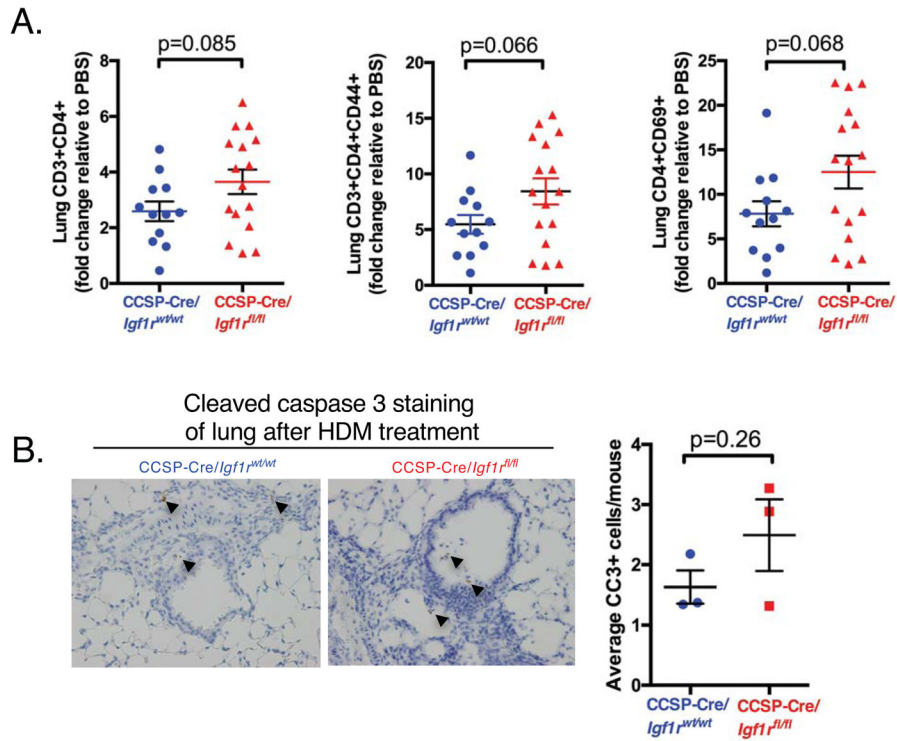
Extended Data Figure 11. IGF-1R expression in alveolar macrophages and airway epithelial cells
Lung sections from wild type mice were stained with antibodies against alveolar macrophages (Mac-2), airway epithelial cells (CC-10), and IGF-1R. (C) is another field showing colocalization of IGF-1R and Mac-2 staining.

LysM-Cre/*Igf1*^{fl/fl} mice

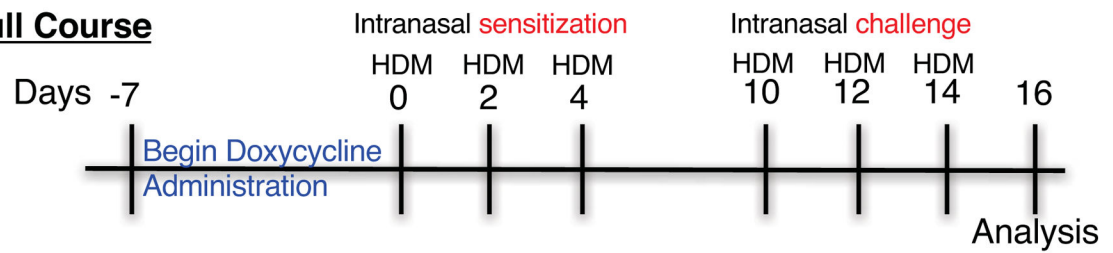
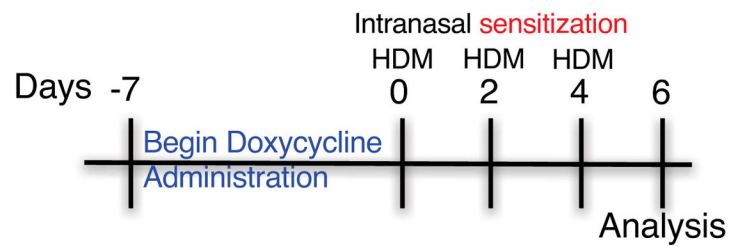
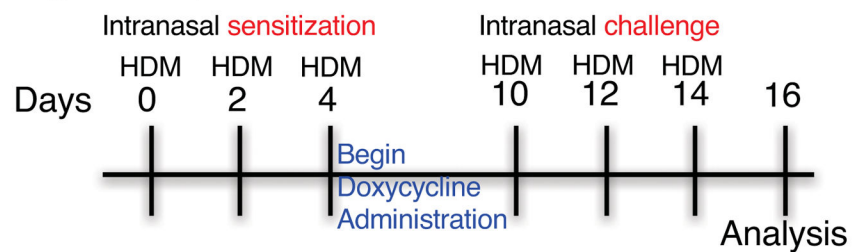


Extended Data Figure 12. Alveolar macrophages from LysM-Cre/*Igf1*^{fl/fl} mice have no detectable *Igf-1* transcript

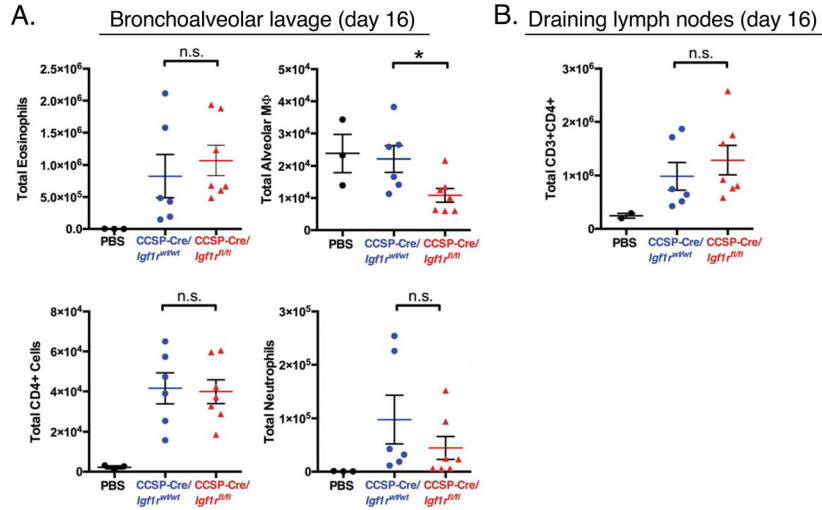
Alveolar macrophages isolated from LysM-Cre/*Igf1*^{fl/fl} and littermate controls were assessed for *Igf-1* mRNA expression (n=2 per group). Data represented as mean ± s.d.



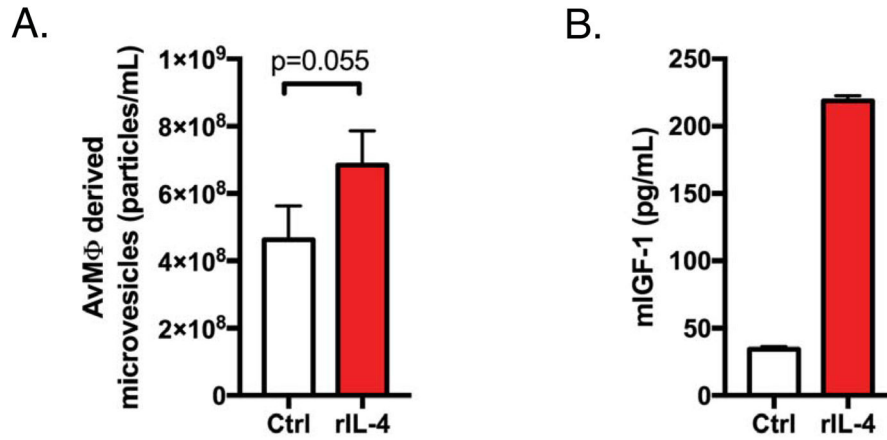
Extended Data Figure 13. CCSP-Cre/Igf1^{fl/fl} mice exposed to HDM show a trend toward greater immune cell infiltration in the lungs and greater apoptotic cells
(A) Total cell counts of lung CD3+ CD4+ T cells (left), CD3+ CD4+ CD44+ T cells (middle), and CD3+ CD4+ CD69+ T-cells (right panel) in the lungs of CCSP-Cre/Igf1^{wt/wt} and Igf1^{fl/fl} mice given the full HDM course. CCSP-Cre/Igf1^{fl/fl} mice exposed to HDM clearly show a trend in increased T-cells in the lung compared to Igf1^{wt/wt} mice, but due to the spread in the data among the many mice analyzed, the data did not achieve statistical significance. **(B)** (left) Representative histology images of cleaved caspase (CC3) staining in lung sections of mice given the full HDM course. Average CC3-positive cells per mouse are quantified on the right (n=3 per group). Black arrowheads indicate positive staining. Data represented as mean ± s.e.m.

Full Course**Regimen #1: Sensitization Phase****Regimen #2: Challenge Phase**

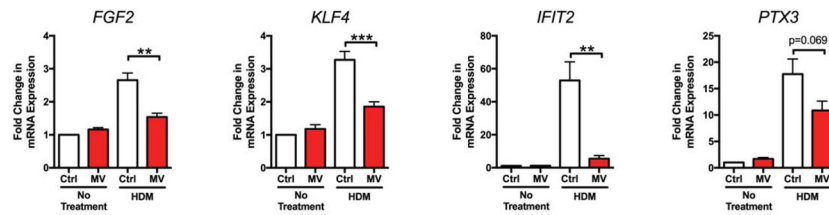
Extended Data Figure 14. Schematic detailing various HDM administration timelines tested
 Schematic describing the different time courses for *Igf1r* deletion from Club cells (induced via administration of doxycycline) and for the allergen HDM exposure.



Extended Data Figure 15. CCSP-Cre/*Igf1*^{wt/wt} and *Igf1*^{fl/fl} mice exposed to HDM for regimen #2 (the challenge phase) have no significant differences in airway inflammation
(A) Total cell counts of various populations in the BAL fluid of CCSP-Cre/*Igf1*^{wt/wt} and CCSP-Cre/*Igf1*^{fl/fl} mice given HDM for regimen #2 (the “challenge phase” time course).
(B) Total cell counts of CD3+ CD4+ T cells of draining lymph nodes of CCSP-Cre/*Igf1*^{wt/wt} and CCSP-Cre/*Igf1*^{fl/fl} mice given HDM for regimen #2 (the “challenge phase” time course). Data represented as mean ± s.e.m.

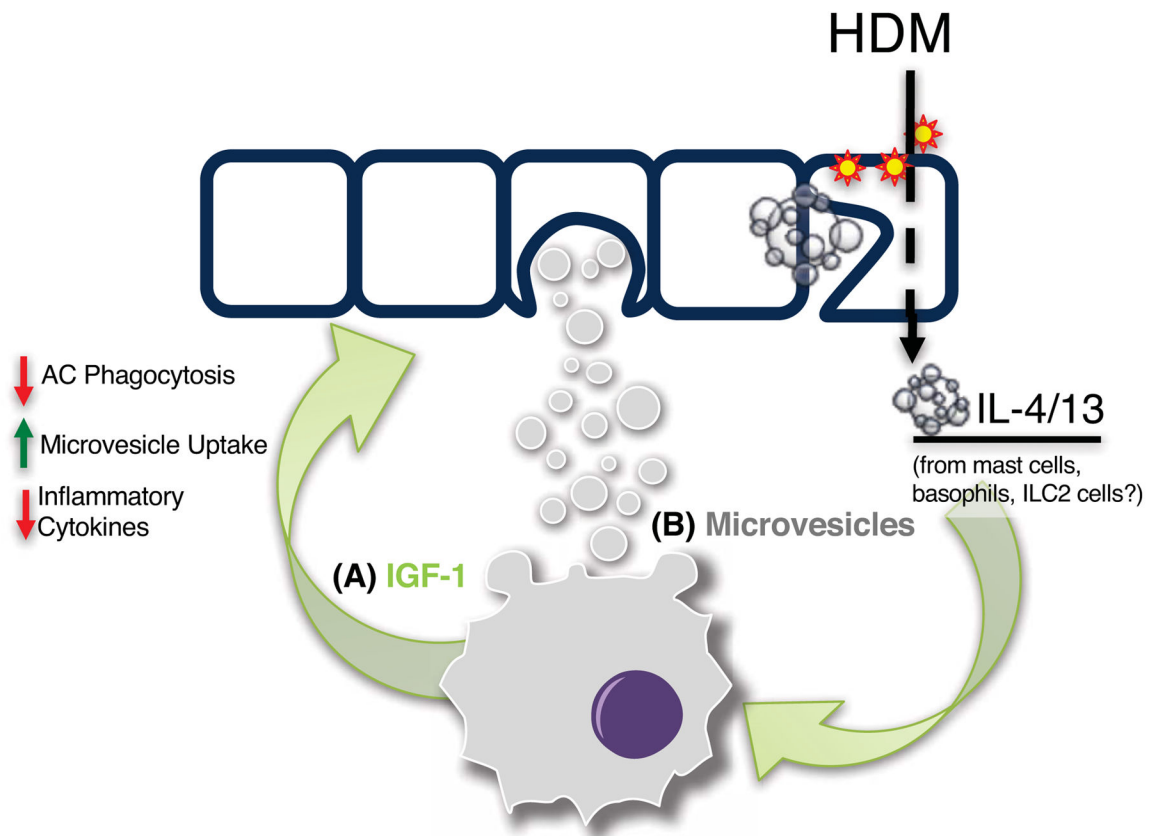


Extended Data Figure 16. Alveolar macrophages exposed to IL-4 produce more microvesicles
(A) Microvesicles were harvested from either control or IL-4 treated MH-S alveolar macrophages and then counted using qNano (n=3) **(B)** Supernatants from (A) were assessed for IGF-1 production by macrophages. Data represented as mean ± s.e.m.



Extended Data Figure 17. Macrophage-derived microvesicles suppress gene expression in lung epithelial cells exposed to house dust mite

BEAS-2B cells were treated with HDM either in the presence or absence of microvesicles isolated from mouse alveolar macrophages for 3 hours and then assessed for expression of *FGF2*, *KLF4*, *IFIT2*, and *PTX3* (n=6). Data represented as mean \pm s.e.m.



Extended Data Figure 18. Potential model of alveolar macrophage and airway epithelial crosstalk

Exposure of airways to allergens, such as HDM, can cause apoptotic cell death as well as IL-4 and IL-13 production, from mast cells and type 2 innate lymphoid cells (ILC2). These cytokines, along with apoptotic cells, trigger alveolar macrophages to produce IGF-1. The released IGF-1 (A) then acts on the airway epithelium to elicit two actions: first, to decrease the uptake of apoptotic cells and second to enhance the uptake of macrophage-derived microvesicles. These microvesicles (B) dampen inflammatory cytokine production by the airway epithelial cells.

Acknowledgments

The authors thank members of the Ravichandran laboratory for discussions and critical reading of manuscript; Sanja Arandjelovic, Kristen Penberthy, and Lisa Haney for scoring histology slides, and Justin Perry for assistance with generation of the heat map, and the UVa flow cytometry core and the UVa Molecular electron microscopy core. This work is supported by grants to K.S.R. from the NIGMS (GM064709), NIMH (MH096484), NHLBI (P01HL120840), and Center for Cell Signaling at the University of Virginia, NHLBI (HL132287 and HL091127) to Y.M.S. Additional support was provided via the NIH Training Grants T32 GM008136 (Cell and Molecular Biology) to C.Z.H.; T32 AI007496 (Immunology) to C.Z.H., M.W.B., and I.J.J.; and T32 GM007267 (MSTP) to M.W.B.

References

1. Nagata S, Hanayama R, Kawane K. Autoimmunity and the clearance of dead cells. *Cell*. 2010; 140:619–630. DOI: 10.1016/j.cell.2010.02.014 [PubMed: 20211132]
2. Henson PM, Hume DA. Apoptotic cell removal in development and tissue homeostasis. *Trends Immunol*. 2006; 27:244–250. DOI: 10.1016/j.it.2006.03.005 [PubMed: 16584921]
3. Burstyn-Cohen T, et al. Genetic dissection of TAM receptor-ligand interaction in retinal pigment epithelial cell phagocytosis. *Neuron*. 2012; 76:1123–1132. DOI: 10.1016/j.neuron.2012.10.015 [PubMed: 23259948]
4. Juncadella IJ, et al. Apoptotic cell clearance by bronchial epithelial cells critically influences airway inflammation. *Nature*. 2013; 493:547–551. DOI: 10.1038/nature11714 [PubMed: 23235830]
5. Wood W, et al. Mesenchymal cells engulf and clear apoptotic footplate cells in macrophageless PU.1 null mouse embryos. *Development*. 2000; 127:5245–5252. [PubMed: 11076747]
6. Lu Z, et al. Phagocytic activity of neuronal progenitors regulates adult neurogenesis. *Nat Cell Biol*. 2011; 13:1076–1083. DOI: 10.1038/ncb2299 [PubMed: 21804544]
7. Ichimura T, et al. Kidney injury molecule-1 is a phosphatidylserine receptor that confers a phagocytic phenotype on epithelial cells. *J Clin Invest*. 2008; 118:1657–1668. DOI: 10.1172/JCI34487 [PubMed: 18414680]
8. Mesa KR, et al. Niche-induced cell death and epithelial phagocytosis regulate hair follicle stem cell pool. *Nature*. 2015; 522:94–97. DOI: 10.1038/nature14306 [PubMed: 25849774]
9. Elliott MR, et al. Unexpected requirement for ELMO1 in clearance of apoptotic germ cells in vivo. *Nature*. 2010; 467:333–337. DOI: 10.1038/nature09356 [PubMed: 20844538]
10. Gregory CD, Pound JD. Microenvironmental influences of apoptosis in vivo and in vitro. *Apoptosis*. 2010; 15:1029–1049. DOI: 10.1007/s10495-010-0485-9 [PubMed: 20237956]
11. Arandjelovic S, Ravichandran KS. Phagocytosis of apoptotic cells in homeostasis. *Nat Immunol*. 2015; 16:907–917. DOI: 10.1038/ni.3253 [PubMed: 26287597]
12. Green DR. The end and after: how dying cells impact the living organism. *Immunity*. 2011; 35:441–444. DOI: 10.1016/j.immuni.2011.10.003 [PubMed: 22035836]
13. Werner S, Grose R. Regulation of wound healing by growth factors and cytokines. *Physiol Rev*. 2003; 83:835–870. DOI: 10.1152/physrev.00031.2002 [PubMed: 12843410]
14. Yakar S, et al. Circulating levels of IGF-1 directly regulate bone growth and density. *J Clin Invest*. 2002; 110:771–781. DOI: 10.1172/JCI15463 [PubMed: 12235108]
15. Firth SM, Baxter RC. Cellular actions of the insulin-like growth factor binding proteins. *Endocr Rev*. 2002; 23:824–854. DOI: 10.1210/er.2001-0033 [PubMed: 12466191]
16. Mulvihill MJ, et al. Discovery of OSI-906: a selective and orally efficacious dual inhibitor of the IGF-1 receptor and insulin receptor. *Future Med Chem*. 2009; 1:1153–1171. DOI: 10.4155/fmc.09.89 [PubMed: 21425998]
17. Garcia-Echeverria C, et al. In vivo antitumor activity of NVP-AEW541-A novel, potent, and selective inhibitor of the IGF-IR kinase. *Cancer Cell*. 2004; 5:231–239. [PubMed: 15050915]
18. Fernandez AM, Torres-Aleman I. The many faces of insulin-like peptide signalling in the brain. *Nat Rev Neurosci*. 2012; 13:225–239. DOI: 10.1038/nrn3209 [PubMed: 22430016]
19. LeRoith D. Insulin-like growth factor I receptor signaling--overlapping or redundant pathways? *Endocrinology*. 2000; 141:1287–1288. DOI: 10.1210/endo.141.4.7475 [PubMed: 10746630]

20. Tosello-Tramont AC, Nakada-Tsukui K, Ravichandran KS. Engulfment of apoptotic cells is negatively regulated by Rho-mediated signaling. *J Biol Chem.* 2003; 278:49911–49919. DOI: 10.1074/jbc.M306079200 [PubMed: 14514696]
21. Leverrier Y, Ridley AJ. Requirement for Rho GTPases and PI 3-kinases during apoptotic cell phagocytosis by macrophages. *Curr Biol.* 2001; 11:195–199. [PubMed: 11231156]
22. Tosello-Tramont AC, Brugnera E, Ravichandran KS. Evidence for a conserved role for CRKII and Rac in engulfment of apoptotic cells. *J Biol Chem.* 2001; 276:13797–13802. DOI: 10.1074/jbc.M011238200 [PubMed: 11297528]
23. Schlam D, et al. Phosphoinositide 3-kinase enables phagocytosis of large particles by terminating actin assembly through Rac/Cdc42 GTPase-activating proteins. *Nat Commun.* 2015; 6:8623. [PubMed: 26465210]
24. Casella JF, Flanagan MD, Lin S. Cytochalasin D inhibits actin polymerization and induces depolymerization of actin filaments formed during platelet shape change. *Nature.* 1981; 293:302–305. [PubMed: 7196996]
25. Yarmola EG, Somasundaram T, Boring TA, Spector I, Bubb MR. Actin-latrunculin A structure and function. Differential modulation of actin-binding protein function by latrunculin A. *J Biol Chem.* 2000; 275:28120–28127. DOI: 10.1074/jbc.M004253200 [PubMed: 10859320]
26. Hetrick B, Han MS, Helgeson LA, Nolen BJ. Small molecules CK-666 and CK-869 inhibit actin-related protein 2/3 complex by blocking an activating conformational change. *Chem Biol.* 2013; 20:701–712. DOI: 10.1016/j.chembiol.2013.03.019 [PubMed: 23623350]
27. Chen F, et al. An essential role for TH2-type responses in limiting acute tissue damage during experimental helminth infection. *Nat Med.* 2012; 18:260–266. DOI: 10.1038/nm.2628 [PubMed: 22245779]
28. Wynes MW, Frankel SK, Riches DW. IL-4-induced macrophage-derived IGF-I protects myofibroblasts from apoptosis following growth factor withdrawal. *J Leukoc Biol.* 2004; 76:1019–1027. DOI: 10.1189/jlb.0504288 [PubMed: 15316031]
29. Ginhoux F, Williams M. Tissue-Resident Macrophage Ontogeny and Homeostasis. *Immunity.* 2016; 44:439–449. DOI: 10.1016/j.immuni.2016.02.024 [PubMed: 26982352]
30. Perl AK, Tichelaar JW, Whitsett JA. Conditional gene expression in the respiratory epithelium of the mouse. *Transgenic Res.* 2002; 11:21–29. [PubMed: 11874100]
31. Wills-Karp M. Interleukin-13 in asthma pathogenesis. *Curr Allergy Asthma Rep.* 2004; 4:123–131. [PubMed: 14769261]
32. Hilton DJ, et al. Cloning and characterization of a binding subunit of the interleukin 13 receptor that is also a component of the interleukin 4 receptor. *Proc Natl Acad Sci U S A.* 1996; 93:497–501. [PubMed: 8552669]
33. Liu JL, Yakar S, LeRoith D. Conditional knockout of mouse insulin-like growth factor-1 gene using the Cre/loxP system. *Proc Soc Exp Biol Med.* 2000; 223:344–351. [PubMed: 10721003]
34. Liu JL, et al. Insulin-like growth factor-I affects perinatal lethality and postnatal development in a gene dosage-dependent manner: manipulation using the Cre/loxP system in transgenic mice. *Mol Endocrinol.* 1998; 12:1452–1462. DOI: 10.1210/mend.12.9.0162 [PubMed: 9731712]
35. Thomas WR, Hales BJ, Smith WA. House dust mite allergens in asthma and allergy. *Trends Mol Med.* 2010; 16:321–328. DOI: 10.1016/j.molmed.2010.04.008 [PubMed: 20605742]
36. Dietrich P, Dragatsis I, Xuan S, Zeitlin S, Efstratiadis A. Conditional mutagenesis in mice with heat shock promoter-driven cre transgenes. *Mamm Genome.* 2000; 11:196–205. [PubMed: 10723724]
37. Perl AK, Zhang L, Whitsett JA. Conditional expression of genes in the respiratory epithelium in transgenic mice: cautionary notes and toward building a better mouse trap. *Am J Respir Cell Mol Biol.* 2009; 40:1–3. DOI: 10.1165/rcmb.2008-0011ED [PubMed: 19075182]
38. Hahn YS, et al. V gamma 4+ gamma delta T cells regulate airway hyperreactivity to methacholine in ovalbumin-sensitized and challenged mice. *J Immunol.* 2003; 171:3170–3178. [PubMed: 12960345]
39. Townley RG, Horiba M. Airway hyperresponsiveness: a story of mice and men and cytokines. *Clin Rev Allergy Immunol.* 2003; 24:85–110. DOI: 10.1385/CRIAI:24:1:85 [PubMed: 12644720]

40. Lambrecht BN, Hammad H. The immunology of asthma. *Nat Immunol.* 2015; 16:45–56. DOI: 10.1038/ni.3049 [PubMed: 25521684]
41. Marini M, Vittori E, Hollemborg J, Mattoli S. Expression of the potent inflammatory cytokines, granulocyte-macrophage-colony-stimulating factor and interleukin-6 and interleukin-8, in bronchial epithelial cells of patients with asthma. *J Allergy Clin Immunol.* 1992; 89:1001–1009. [PubMed: 1583242]
42. Zhou B, et al. Thymic stromal lymphopoietin as a key initiator of allergic airway inflammation in mice. *Nat Immunol.* 2005; 6:1047–1053. DOI: 10.1038/ni1247 [PubMed: 16142237]
43. Lambrecht BN, Hammad H. The immunology of asthma. *Nat Immunol.* 2014; 16:45–56. DOI: 10.1038/ni.3049
44. Barnes PJ. Immunology of asthma and chronic obstructive pulmonary disease. *Nat Rev Immunol.* 2008; 8:183–192. DOI: 10.1038/nri2254 [PubMed: 18274560]
45. Machado DC, Horton D, Harrop R, Peachell PT, Helm BA. Potential allergens stimulate the release of mediators of the allergic response from cells of mast cell lineage in the absence of sensitization with antigen-specific IgE. *Eur J Immunol.* 1996; 26:2972–2980. DOI: 10.1002/eji.1830261224 [PubMed: 8977293]
46. Huels C, et al. Co-activation of naive CD4+ T cells and bone marrow-derived mast cells results in the development of Th2 cells. *Int Immunol.* 1995; 7:525–532. [PubMed: 7547678]
47. Bradding P, et al. TNF alpha is localized to nasal mucosal mast cells and is released in acute allergic rhinitis. *Clin Exp Allergy.* 1995; 25:406–415. [PubMed: 7553243]
48. Gessner A, Mohrs K, Mohrs M. Mast cells, basophils, and eosinophils acquire constitutive IL-4 and IL-13 transcripts during lineage differentiation that are sufficient for rapid cytokine production. *J Immunol.* 2005; 174:1063–1072. [PubMed: 15634931]
49. Sokol CL, Barton GM, Farr AG, Medzhitov R. A mechanism for the initiation of allergen-induced T helper type 2 responses. *Nat Immunol.* 2008; 9:310–318. DOI: 10.1038/ni1558 [PubMed: 18300366]
50. Sokol CL, Medzhitov R. Role of basophils in the initiation of Th2 responses. *Curr Opin Immunol.* 2010; 22:73–77. DOI: 10.1016/j.coi.2010.01.012 [PubMed: 20144855]
51. Sokol CL, Medzhitov R. Emerging functions of basophils in protective and allergic immune responses. *Mucosal Immunol.* 2010; 3:129–137. DOI: 10.1038/mi.2009.137 [PubMed: 20072123]
52. Bourdonnay E, et al. Transcellular delivery of vesicular SOCS proteins from macrophages to epithelial cells blunts inflammatory signaling. *J Exp Med.* 2015; 212:729–742. DOI: 10.1084/jem.20141675 [PubMed: 25847945]
53. Burger D, et al. Microparticles: biomarkers and beyond. *Clin Sci (Lond).* 2013; 124:423–441. DOI: 10.1042/CS20120309 [PubMed: 23249271]
54. Bissonnette EY, et al. Fibroblast growth factor-2 is a sputum remodeling biomarker of severe asthma. *J Asthma.* 2014; 51:119–126. DOI: 10.3109/02770903.2013.860164 [PubMed: 24188024]
55. Zhang J, et al. Pentraxin 3 (PTX3) expression in allergic asthmatic airways: role in airway smooth muscle migration and chemokine production. *PLoS One.* 2012; 7:e34965. [PubMed: 22529962]
56. Yang IV, et al. The clinical and environmental determinants of airway transcriptional profiles in allergic asthma. *Am J Respir Crit Care Med.* 2012; 185:620–627. DOI: 10.1164/rccm.201108-1503OC [PubMed: 22246175]
57. Chamberland A, Madore AM, Tremblay K, Laviolette M, Laprise C. A comparison of two sets of microarray experiments to define allergic asthma expression pattern. *Exp Lung Res.* 2009; 35:399–410. [PubMed: 19842841]
58. Yakar S, Liu JL, Le Roith D. The growth hormone/insulin-like growth factor-I system: implications for organ growth and development. *Pediatr Nephrol.* 2000; 14:544–549. [PubMed: 10912516]
59. Musaro A, et al. Localized Igf-1 transgene expression sustains hypertrophy and regeneration in senescent skeletal muscle. *Nat Genet.* 2001; 27:195–200. DOI: 10.1038/84839 [PubMed: 11175789]
60. Kenyon CJ. The genetics of ageing. *Nature.* 2010; 464:504–512. DOI: 10.1038/nature08980 [PubMed: 20336132]

61. Lin K, Hsin H, Libina N, Kenyon C. Regulation of the *Caenorhabditis elegans* longevity protein DAF-16 by insulin/IGF-1 and germline signaling. *Nat Genet.* 2001; 28:139–145. DOI: 10.1038/88850 [PubMed: 11381260]
62. Gasparini L, Xu H. Potential roles of insulin and IGF-1 in Alzheimer's disease. *Trends Neurosci.* 2003; 26:404–406. DOI: 10.1016/S0166-2236(03)00163-2 [PubMed: 12900169]
63. Smith TJ. Insulin-like growth factor-I regulation of immune function: a potential therapeutic target in autoimmune diseases? *Pharmacol Rev.* 2010; 62:199–236. DOI: 10.1124/pr.109.002469 [PubMed: 20392809]
64. Yeager M, Berriman JA, Baker TS, Bellamy AR. Three-dimensional structure of the rotavirus haemagglutinin VP4 by cryo-electron microscopy and difference map analysis. *EMBO J.* 1994; 13:1011–1018. [PubMed: 8131735]

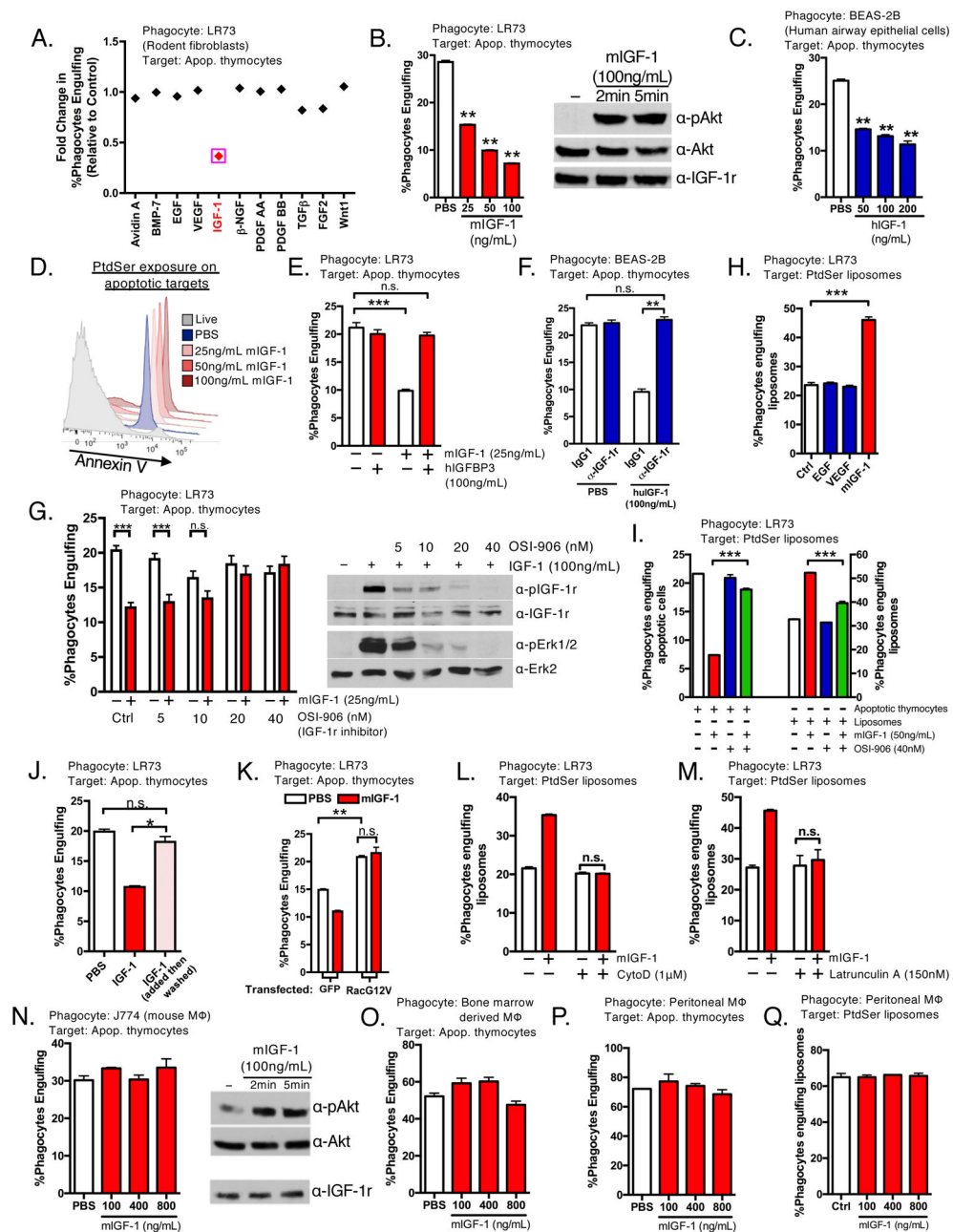


Figure 1. IGF-1 dampens apoptotic cell engulfment and enhances liposome uptake by non-professional phagocytes

a, Effect of 11 growth factors on apoptotic cell engulfment by LR73 cells (each normalized to vehicle control). **b,** (Left) Engulfment by LR73 cells treated with increasing concentrations of IGF-1. (Right) Immunoblotting for IGF-1R and Akt phosphorylation. **c,** Apoptotic cell uptake by BEAS-2B cells treated with human IGF-1. **d,** IGF-1 does not affect Annexin V binding to apoptotic thymocytes ($n=6$). **e, f,** Reversal of IGF-1 mediated engulfment inhibition of LR73 cells by IGBFP3 (**e**), or BEAS-2B epithelial cells by IGF-1R neutralizing antibody (**f**). **g,** IGF-1-mediated reduction in engulfment is reversed by the IGF-1R inhibitor OSI-906 (left), and immunoblotting for IGF-1R and Erk1/2

phosphorylation (right). **h**, Liposome uptake by LR73 cells treated with either IGF-1 (50ng/mL), EGF or VEGF (100ng/mL each). **i**, Enhanced liposome uptake by IGF-1 is reversed by OSI-906. **j**, LR73 cells pretreated with IGF-1 were washed, and incubated with apoptotic thymocytes in the presence or absence of IGF-1. **k**, Engulfment by LR73 cells transfected with RacG12V treated and with mIGF-1. **l, m**, Engulfment by LR73 cells treated with Cytochalasin D (**l**) or Latrunculin A (**m**) and incubated with liposomes with or without IGF-1. **n**, (Left) Phagocytosis of apoptotic thymocytes by J774 macrophage cells treated with IGF-1. (Right) Immunoblotting for IGF-1R expression and Akt phosphorylation. **o, p**, Apoptotic cell engulfment by bone marrow derived macrophages or resident peritoneal macrophages treated with IGF-1. **q**, Liposome uptake by resident peritoneal macrophages treated with IGF-1. For **a–q**, except **d**, n=3; representative experiment is shown and data are mean \pm s.d. n.s.- not significant. *p*-value of <0.05 (*), <0.01 (**), or <0.001 (***). See Supplementary Figure 1 for uncropped immunoblots.

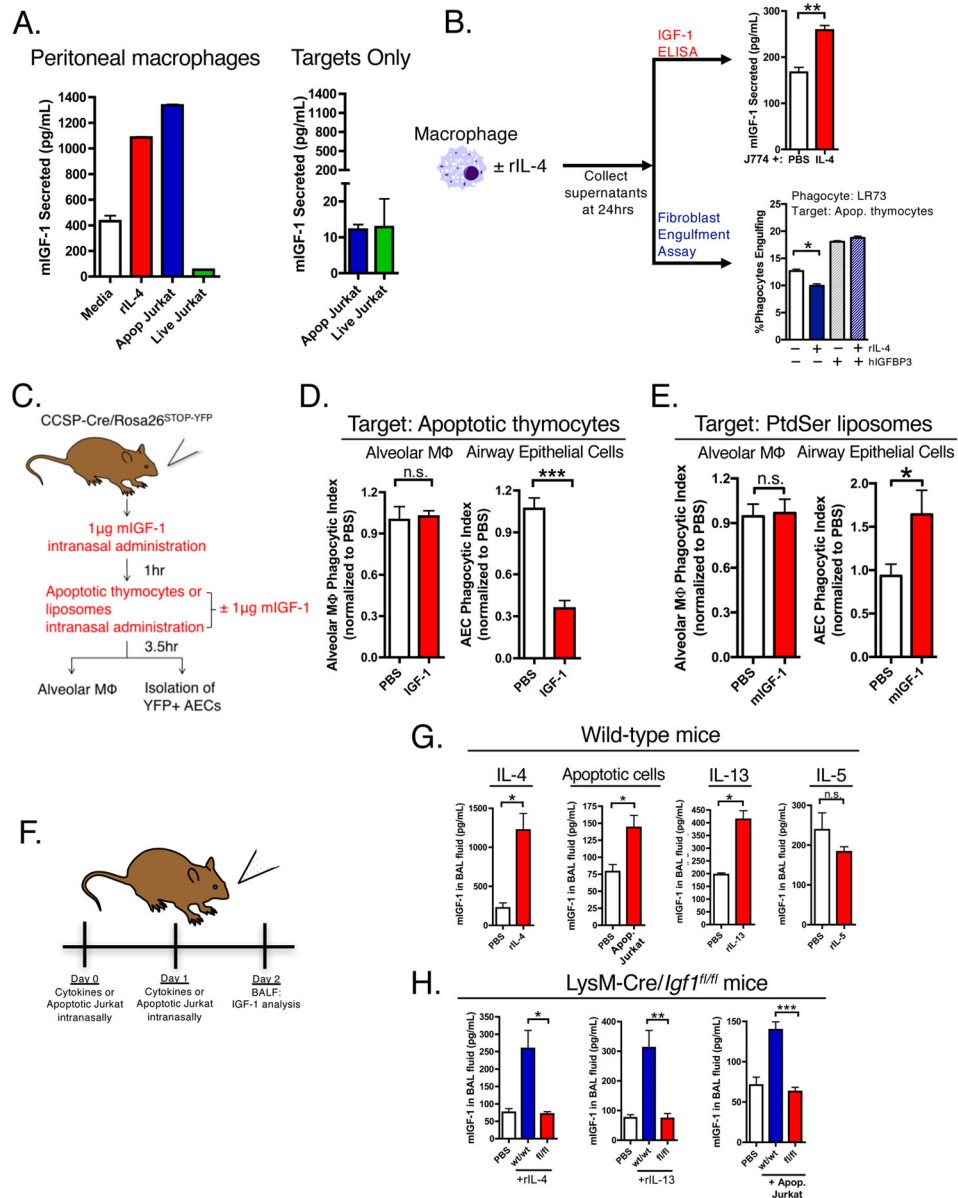


Figure 2. Macrophages produce IGF-1 during apoptotic cell clearance

a. (Left) IGF-1 secretion by peritoneal macrophages stimulated with IL-4, apoptotic Jurkat cells or live Jurkat cells. (Right) Apoptotic or live Jurkat cells do not produce IGF-1 (representative of $n=3$), mean \pm s.d. **b.** J774 cells were treated with rIL-4. After 24hrs, half of the supernatant was assessed for IGF-1 secretion by ELISA, (right panel) and the other half was incubated with PBS or IGBP3 and then tested in the phagocytosis using LR73 cells (right) (representative of $n=3$), mean \pm s.d. Note: addition of IGFBP3 increases the basal phagocytosis due to low basal levels of IGF-1 found in the supernatant of unstimulated J774 cells. **c, d, e.** CCSP-Cre mice with YFP⁺ Club cells were pre-treated with 1 μ g IGF-1 intranasally for 1hr and then administered targets with or without IGF-1. Uptake of apoptotic thymocytes (**d**, $n=6$ per group) or liposomes (**e**, $n=3$ per group) by alveolar macrophages and lung epithelial cells were then assessed. **f.** Wild-type mice were given PBS, IL-4, apoptotic

cells, IL-5, or IL-13 intranasally for 2 consecutive days, and the BAL fluid assessed for IGF-1 (n=2–3 mice per group for cytokines, n=5, 8 for apoptotic cell instillation). **g.** LysM-Cre/*Igf1*^{wt/wt} or *Igf1*^{fl/fl} mice were given PBS, IL-4 or IL-13, or apoptotic cells intranasally, and BAL fluid assessed for IGF-1 (n=6, 6, 4 mice per group for rIL-4; n=6, 4, 4 for rIL-13; n=6, 9, 9 mice per group for apoptotic cell instillation). Data are mean ± s.e.m unless otherwise indicated.

Author Manuscript

Author Manuscript

Author Manuscript

Author Manuscript

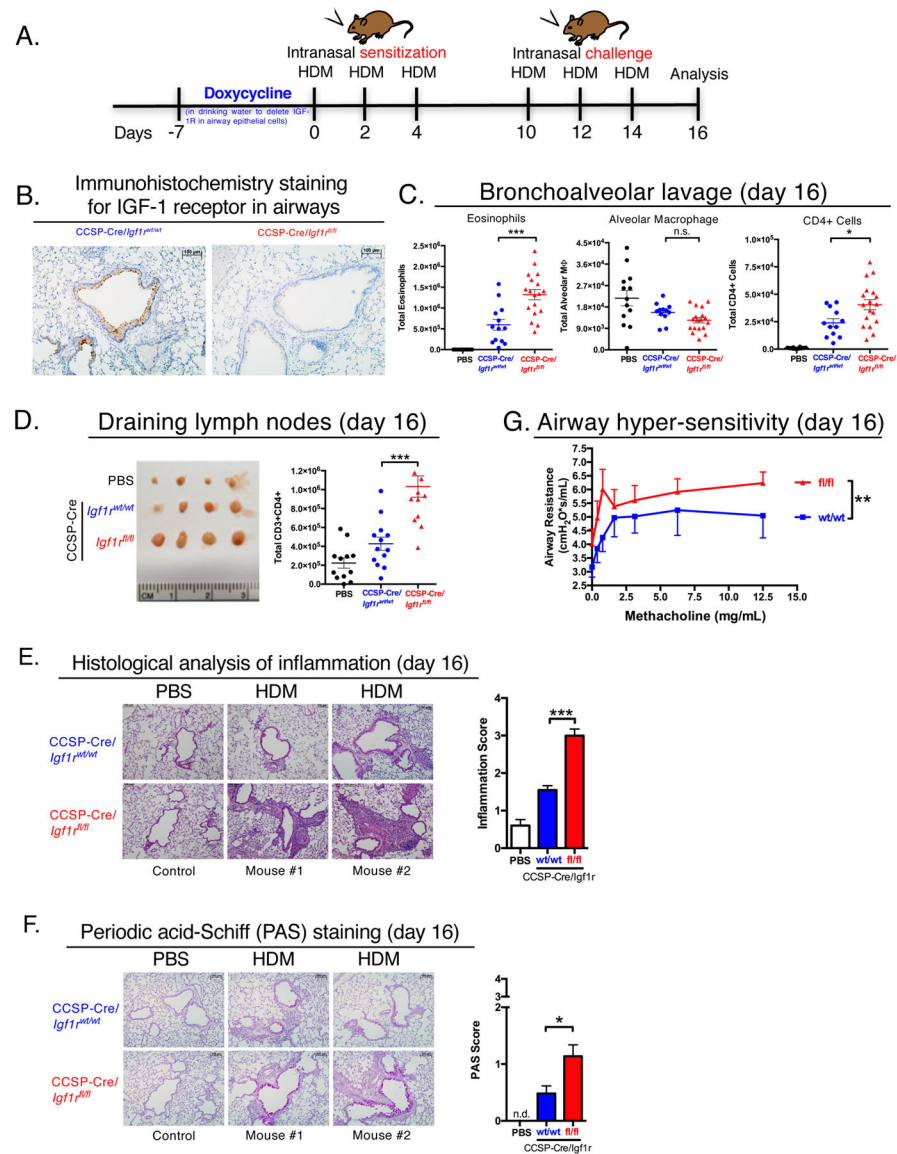


Figure 3. Mice lacking IGF-1R in airway epithelial cells have exacerbated airway inflammation

a, Schematic of HDM induced allergic airway inflammation. **b**, Representative images showing IGF-1R expression in bronchial epithelial cells, and its loss in *CCSP-^{trTA/tetO-Cre}/Igf1^{fl/fl}* mice treated with doxycycline. **c**, Numbers of eosinophils, alveolar macrophages, and CD4⁺ T cells in the BAL fluid of *CCSP-Cre/Igf1^{wt/wt}* and *Igf1^{fl/fl}* mice administered PBS or HDM (each dot represents a mouse). **d**, (Left) Representative lung draining lymph nodes from *CCSP-Cre/Igf1^{wt/wt}* and *CCSP-Cre/Igf1^{fl/fl}* mice that were given PBS or HDM. (Right) Total CD4⁺ T cell counts from lymph nodes. **e**, **f**, **g**, **h**, Representative hematoxylin and eosin (H&E) images (**e**) or PAS staining (**g**) of lung sections from *CCSP-Cre/Igf1^{wt/wt}* and *CCSP-Cre/Igf1^{fl/fl}* mice given PBS or HDM (n=3–4 mice per condition). Representative histological scoring of inflammation (**f**) and PAS staining (**h**) (n=6–10 sections and 3 mice per condition). All data are presented as mean ± s.e.m.

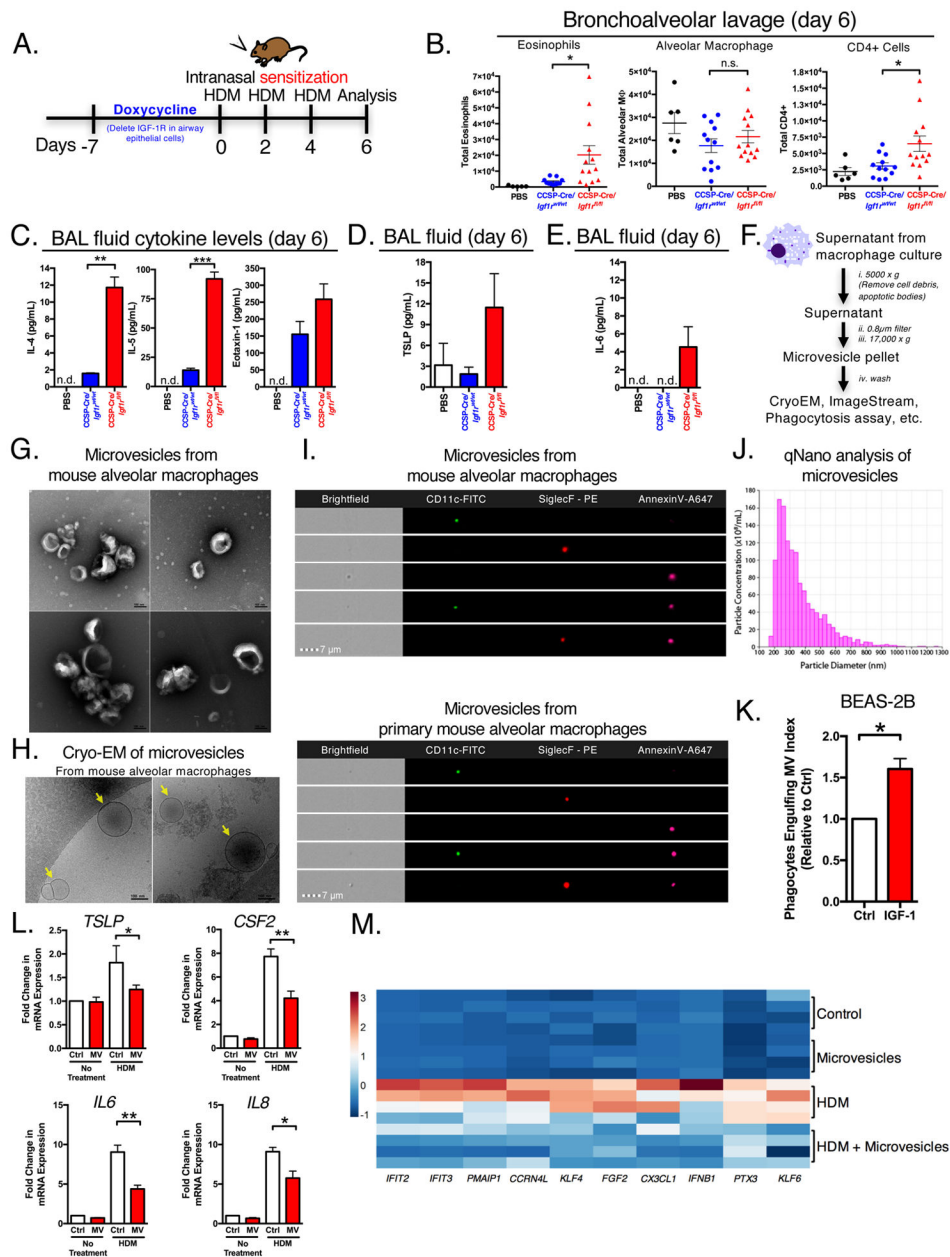


Figure 4. IGF-1R expression in airway epithelial cells is required in the sensitization phase of airway inflammation

a, Schematic of IGF-1R deletion prior to the sensitization phase to assess its effect on early stages of inflammation. **b**, Numbers of eosinophils, alveolar macrophages, and CD4⁺ T cells in the BAL of CCSP-Cre/*Igf1^{wt/wt}* and CCSP-Cre/*Igf1^{fl/fl}* mice primed with PBS or HDM. **c**, **d**, **e**, Analysis of IL-4, IL-5, eotaxin-1, and IL-6 (via Luminex **c**, **e**, n=3 mice per group) and TSLP (by ELISA, **d**, n=2, 7, 9 mice per group) in the BAL fluid from representative CCSP-Cre/*Igf1^{wt/wt}* and CCSP-Cre/*Igf1^{fl/fl}* mice primed with PBS or HDM. **f**, Schematic of generation and isolation of alveolar macrophage derived microvesicles. **g**, **h**, Representative negative-stain EM (**g**) or cryo-EM (**h**) images of microvesicles isolated from mouse alveolar macrophages. Images show spherical membrane-bound structures of a range

of sizes (yellow arrows). **i**, ImageStreamX™ analysis of microvesicles isolated from mouse alveolar macrophage cell line and primary mouse alveolar macrophages and stained for representative alveolar macrophage markers. **j**, Tunable resistive pulse sensing analysis of microvesicles from alveolar macrophages using qNano, pore size 400nm, to determine frequency and sizing of microvesicles (representative of n=3). **k**, BEAS-2B cells treated with IGF-1 (100ng/mL) were assessed for uptake of alveolar macrophage derived microvesicles (n=4). **l**, BEAS-2B cells were treated with HDM either in the presence or absence of alveolar macrophage derived microvesicles for 3 hours and assessed for expression of *TSLP*, *CSF2*, *IL6*, *IL8* (n=4). **m**, Heatmap of top 10 differentially expressed genes from RNA-seq analysis of BEAS-2B cells exposed to HDM with or without alveolar macrophage-derived microvesicles. Data presented as mean ± s.e.m. n.d. is not detected